Practical Nonlinear Flight Dynamic Modeling for Multirotor Aircraft

Jeremy W. Hopwood*
Mississippi State University, Mississippi State, MS 39762

Benjamin M. Simmons† and Craig A. Woolsey‡
Virginia Tech, Blacksburg, VA 24061

Jared K. Cooper§
Barron Associates, Inc., Charlottesville, VA 22901

High-fidelity yet compact nonlinear flight dynamic models for multirotor aircraft are derived from blade-element and momentum theory for use in control, estimation, and efficient simulation. The aim is to obtain models that are valid over a wide range of flight conditions and identifiable from flight data. Individual rotor force and moment models along with airframe aerodynamics and motor inertial effects are incorporated into a quasi-steady, nonlinear model for generic multirotor aircraft. A simulation study is conducted in which the derived model is used to inform the design of statistically principled experiments that facilitate accurate model identification. The relative importance of model parameters is evaluated using a high-fidelity simulation constructed from wind tunnel data. This process informs the selection and estimation of model parameters, which are then used to quantify the contribution of model terms across common flight conditions.

I. Introduction

Flight dynamic models for aircraft are often required for control, estimation, simulation, and design. Formulating flight dynamic models as low-dimensional systems of ordinary differential equations allows for direct use in control and estimation algorithms as well as efficient simulation and design optimization [1, 2]. Higher-fidelity models based on computational or wind tunnel data are not practical in such applications. Hence, this paper details the development of nonlinear, quasi-steady flight dynamic models for multirotor aircraft that balance complexity and accuracy to enable identification from flight data and subsequent model-based controller and estimator design.

There is no standard structure for compact, finite-dimensional models for full-envelope multirotor aircraft flight, though significant progress has been made in this area for fixed-wing aircraft [3–5]. Large-domain modeling for multirotor aircraft is especially challenging due to complex inflow conditions [6], unsteady effects [7], and aerodynamic interactions [8]. Therefore, typical approaches to multirotor modeling for the purposes of control and estimation involve identifying linear state space models in the time domain or low-order transfer functions in the frequency domain [9–14]. Although these approaches enable a multitude of control and estimation approaches, incorporating an aerodynamic model that is more accurate over a broader envelope can yield stronger guarantees on safety and performance.

Approaches to expand the range of flight conditions for which a model accurately describes multirotor motion include stitched linear models [15], linear force and moment models for the otherwise nonlinear system [16], reduced-dimensional nonlinear aerodynamic models that leverage symmetry [17], and polynomial-based regressor determination using stepwise regression [18]. These models are valid across a wider range of flight conditions than linear flight dynamic models. Incorporating known physics into the model structure, however, can further improve the model's utility and interpretability. Such an approach often begins with the aerodynamics of a single rotor whose effects are superposed to obtain a final multirotor model structure [11, 19, 20]. Despite these advancements, existing physics-based approaches are typically constrained to a limited range of flight conditions. A model that is valid within a larger domain, accurately capturing nonlinear dynamic and aerodynamic phenomena, may be required for applications of interest. For example, the recent growth in urban air mobility has spawned novel vertical takeoff and landing vehicle designs, motivating physics-based, analytical models such as the one detailed by Nguyen and Webb [21]. While these models describe the complex phenomena driving the vehicle motion, they require a high-dimensional system representation, making identification and control difficult. There is a need for an intermediate fidelity approach in which a physics-based, nonlinear, quasi-steady flight dynamic model can be identified from flight data.

This paper presents a nonlinear, quasi-steady multirotor aerodynamic model that is accurate over a wider range of flight conditions than typical control-oriented models, yet simpler to identify and apply in model-based design compared to models that interpolate extensive archives of experimental or computational data. Similar to Fay [22], the approach begins by deriving the force and moment generated by a single rotor in forward flight using blade-element theory and momentum theory. The resulting lumped-parameter force and moment models for a single rotor are then superposed across multiple rotors to represent the force and moment acting on

---

This is the accepted manuscript of an article published in the *Journal of Aircraft*. The version of record is available at `https://doi.org/10.2514/1.C038103`.

*Assistant Professor, Department of Aerospace Engineering, Member AIAA
†Research Affiliate, Kevin T. Crofton Department of Aerospace and Ocean Engineering; also Research Engineer, Flight Dynamics Branch, NASA Langley Research Center; Member AIAA
‡Professor, Kevin T. Crofton Department of Aerospace and Ocean Engineering, Associate Fellow AIAA
§Senior Research Scientist, Senior Member AIAA

a translating and rotating multirotor aircraft. The final nonlinear model is broadly applicable and amenable to identification from experimental data. Recognizing that simplified models remain useful in certain applications, a set of reasonable assumptions is provided to simplify the model structure and make the parameter estimation problem easier.

To evaluate the effectiveness of the postulated multirotor model structure, a simulation study was conducted using a high-fidelity multirotor aerodynamic model derived from wind tunnel data [23]. A statistically designed test matrix [24, 25] was developed to facilitate accurate identification of the model terms in each model structure. The models are assessed using prediction error metrics and comparisons of the model predictions to the known simulation database, which reveals the advantages and limitations of each modeling approach. The results indicate the relative importance of model terms across a large domain of interest.

The remainder of this paper is as follows. Section II derives lumped-parameter expressions for the aerodynamic force and moment acting on a single rotor in forward flight using blade-element and momentum theory. The result is used in Section III to formulate the total force and moment for a rotating and translating multirotor aircraft. Section IV describes the simulation study, followed by modeling results presented in Section V. Conclusions are discussed in Section VI.

II. Rotor Aerodynamics

A major objective in this paper is to model the aerodynamic force $\boldsymbol{F}$ and moment $\boldsymbol{M}$ acting on a multirotor aircraft in a way that captures the propulsion physics accurately enough to support effective model-based design of nonlinear control and estimation schemes, but is simple enough to allow straightforward model parameter estimation. Let $\boldsymbol{v} = [u\ v\ w]^\mathsf{T}$ and $\boldsymbol{\omega} = [p\ q\ r]^\mathsf{T}$ be the translational and angular velocities of the aircraft, respectively, expressed in a body-fixed frame $\{\boldsymbol{b}_1, \boldsymbol{b}_2, \boldsymbol{b}_3\}$ located at the aircraft's center of gravity (CG). The vectors $\boldsymbol{b}_1$, $\boldsymbol{b}_2$, and $\boldsymbol{b}_3$ form a right-handed orthonormal triad, where $\boldsymbol{b}_1$ points out the front of the aircraft, $\boldsymbol{b}_2$ out the right-hand side, and $\boldsymbol{b}_3$ out the bottom. We aim to derive a model for $\boldsymbol{F}$ and $\boldsymbol{M}$ as functions of the vehicle's velocity and propulsor states, where the propulsors are assumed to be fixed-pitch, rigid rotors. The aerodynamics of these rotors serve as the building block that will define the aerodynamic force and moment acting on the multirotor aircraft.

Consider an N_b-blade rotor of radius R, rotating at a constant angular rate Ω about its spin axis and steadily translating through still air with velocity $\boldsymbol{v}$ and airspeed $V = \|\boldsymbol{v}\|$.

Assumption 1 *The blade-element loads are steady, depending only on the translational velocity of the rotor hub and the rotor rotational speed.*

In other words, the effect of rotor angular velocity orthogonal to the shaft on the blade element angle-of-attack is neglected. Note, however, that the vehicle's angular velocity $\boldsymbol{\omega}$ is not entirely ignored; as detailed in Section III, it will be used to compute the rotor hub's local translational velocity, thereby yielding a quasi-steady aerodynamic model.

To simplify the discussion of rotor aerodynamics, we assume for the time being that the "aircraft" comprises a single rotor located at the origin of the body frame with the rotor spin axis aligned with $\boldsymbol{b}_3$. Referring to Figure 1, let orthonormal vectors $\{\boldsymbol{r}_1, \boldsymbol{r}_2, \boldsymbol{r}_3\}$ define a reference frame centered at the rotor hub such that

a) $\boldsymbol{r}_3 = -\boldsymbol{b}_3$;
b) if $\|\boldsymbol{v}\| > 0$, then $\boldsymbol{v}$ lies in the $\boldsymbol{r}_1$-$\boldsymbol{r}_3$ plane such that $\boldsymbol{r}_1^\mathsf{T}\boldsymbol{v} > 0$;
c) if $\|\boldsymbol{v}\| = 0$, then $\boldsymbol{r}_1 = \boldsymbol{b}_1$;
d) $\boldsymbol{r}_2$ completes a right-handed frame.

The rotor frame is defined similar to the wind frame for fixed-wing aircraft in the sense that the frame axes are defined by the air-relative velocity vector. The rotor frame is related to the body frame by the transformation

$$\boldsymbol{R}_\mathrm{BR} = \begin{bmatrix} \cos\beta_f & -\sin\beta_f & 0 \\ -\sin\beta_f & -\cos\beta_f & 0 \\ 0 & 0 & 1 \end{bmatrix} \tag{1}$$

where β_f is the angle from $\boldsymbol{r}_1$ to $\boldsymbol{b}_1$, measured about the $\boldsymbol{r}_3$ axis. Note that $\boldsymbol{R}_\mathrm{BR}$ is not a proper rotation matrix. In the rotor frame, the velocity of the rotor hub is $\tilde{\boldsymbol{v}} = [v_x\ \ 0\ \ v_z]^\mathsf{T}$, where v_z is the *rotor ascent speed* and v_x is the *rotor-plane airspeed.* Referring to Figure 1, for a non-rotating body frame ($\boldsymbol{\omega} = \boldsymbol{0}$), the matrix $\boldsymbol{R}_\mathrm{BR}$ defines the relations

$$\begin{bmatrix} u \\ v \\ w \end{bmatrix} = \boldsymbol{R}_\mathrm{BR}\tilde{\boldsymbol{v}} = \begin{bmatrix} v_x\cos\beta_f \\ -v_x\sin\beta_f \\ -v_z \end{bmatrix} \tag{2}$$

and

$$\begin{bmatrix} v_x \\ 0 \\ v_z \end{bmatrix} = \boldsymbol{R}_\mathrm{BR}^\mathsf{T}\boldsymbol{v} = \begin{bmatrix} u\cos\beta_f - v\sin\beta_f \\ -u\sin\beta_f - v\cos\beta_f \\ -w \end{bmatrix} \tag{3}$$

By the definition of the rotor frame, v_x also satisfies

$$v_x = \sqrt{u^2 + v^2} \geq 0 \tag{4}$$

Figure 1 depicts the relationship between the body and rotor frames along with the respective components of the velocity vector, $\boldsymbol{v}$, in this special case where we have assumed the rotor hub coincides with the aircraft CG. In Figure 1, $\boldsymbol{v}$ is depicted with $u < 0$, $v > 0$, and $w < 0$. Also note in this case that $v_z > 0$ and $\beta_f > 0$.

The non-dimensional *horizontal advance ratio* is

$$\mu_x = \frac{v_x}{\Omega R} \tag{5}$$

In a similar manner, the *total inflow ratio* is

$$\lambda = \frac{\nu + v_z}{\Omega R} \tag{6}$$

where ν is the induced rotor inflow velocity (positive in the $\boldsymbol{b}_3$ direction). For the purpose of rotor force and moment derivation, consider the following assumption on the rotor aerodynamics.

Assumption 2 *The rotor blades*

a) *are rigid and rigidly attached to the rotor hub (no flapping or feathering);*
b) *do not stall;*
c) *have linear twist: $\theta(\mathfrak{r}) = \theta_0 + \theta_\mathrm{tw}\mathfrak{r}$, where $\mathfrak{r} \in [0, 1]$ is the non-dimensional radial station along the blade measured from the hub; and*

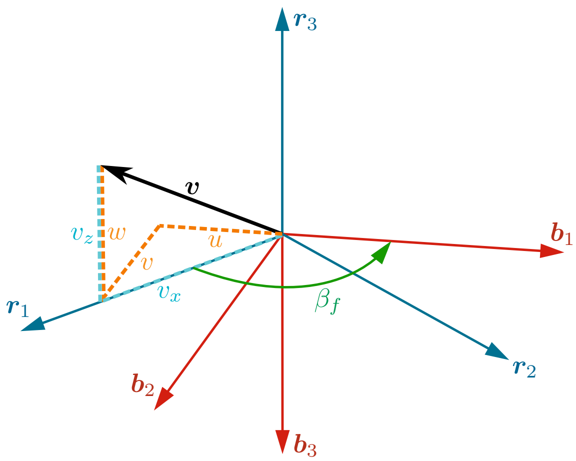

Fig. 1 Rotor frame geometry

d) *do not interact with the wake of upstream blades.*

Consider the thrust T, hub force H, side force S, rolling moment $\mathcal{R}$, pitching moment $\mathcal{P}$, and torque $\mathcal{Q}$ on the isolated rotor shown in Figure 2. Due to Assumptions 2a and 2d, the rotor-frame side force, S, and pitching moment, $\mathcal{P}$, are zero [26, Ch. 5].

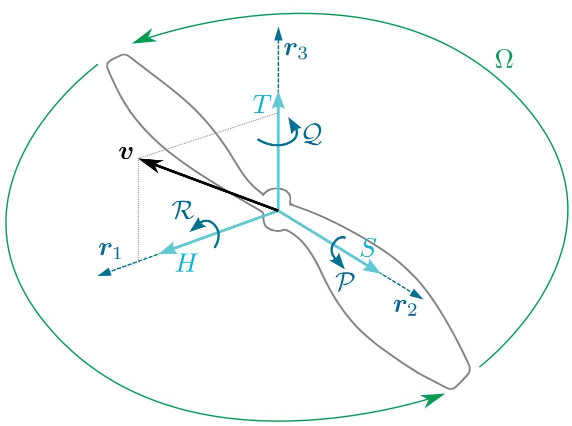

Fig. 2 Isolated rotor force and moment

As detailed in Chapters 4 and 5 of [26], the rotor forces and moments can be obtained by integrating the force and moment acting on an infinitesimal element of the rotor blade. It is convenient to express these quantities as the non-dimensional coefficients,

$$C_H = \frac{H}{\rho\pi R^4\Omega^2} \quad C_T = \frac{T}{\rho\pi R^4\Omega^2}$$
$$C_{\mathcal{R}} = \frac{\mathcal{R}}{\rho\pi R^5\Omega^2} \quad C_{\mathcal{Q}} = \frac{\mathcal{Q}}{\rho\pi R^5\Omega^2} \tag{7}$$

where ρ is the air density. Denote the constant lift curve slope of a blade element as a, its mean drag coefficient as $\bar{c}_d$ (computed at $\mathfrak{r} = \sqrt{2}/2$), and the mean chord length as $\bar{c}$. The rotor force and moment coefficients are given as

$$C_H = -\frac{N_\mathrm{b}\bar{c}a}{2\pi R}\left[\frac{1}{2a}\bar{c}_d\mu_x + \left(\frac{\theta_0}{2} + \frac{\theta_\mathrm{tw}}{4}\right)\lambda\mu_x\right] \tag{8a}$$
$$C_T = \frac{N_\mathrm{b}\bar{c}a}{2\pi R}\left[\frac{\theta_0}{3}\left(1 + \frac{3}{2}\mu_x^2\right) + \frac{\theta_\mathrm{tw}}{4}\left(1 + \mu_x^2\right) - \frac{\lambda}{2}\right] \tag{8b}$$
$$C_{\mathcal{R}} = -\frac{N_\mathrm{b}\bar{c}a}{2\pi R}\left[\frac{\theta_0}{3} + \frac{\theta_\mathrm{tw}}{4} - \frac{\lambda}{4}\right]\mu_x \tag{8c}$$
$$C_{\mathcal{Q}} = -\frac{N_\mathrm{b}\bar{c}a}{2\pi R}\left[\frac{\bar{c}_d}{4a}\left(1 + \mu_x^2\right) + \left(\frac{\theta_0}{3} + \frac{\theta_\mathrm{tw}}{4} - \frac{\lambda}{2}\right)\lambda\right] \tag{8d}$$

These coefficients are similarly derived in [22] and [1] as applied to multirotor vehicles. Various additional contributions to the aerodynamic force on a blade element are accounted for by Johnson [26, §11-6], including the hub's translational velocity, the rotor shaft's pitch and roll velocity, and blade flapping. While we do not account for these perturbations here, one may include them to increase the model's fidelity.

An explicit expression for the induced rotor inflow velocity ν is still needed to determine the inflow ratio λ given in Eq. (6). From momentum theory [27, Ch. 2], the inflow velocity in hover is

$$\nu_0 = \sqrt{\frac{mg}{2\rho A_\mathrm{r}}} \tag{9}$$

where A_r is the total rotor disk area of the aircraft. However, we are interested in the more general forward flight condition where the steady, uniform inflow velocity is implicitly defined by

$$\nu = \frac{\nu_0^2}{\sqrt{v_x^2 + (\nu + v_z)^2}} \tag{10}$$

To simplify the dependence on v_x and v_z, we choose to linearly approximate the curvy surface defined by Eq. (10) with a plane in the ν-v_x-v_z space.

Assumption 3 *The rotor inflow velocity is steady and uniform, given by*

$$\nu = \nu_0 - C_{\nu_x}v_x - C_{\nu_z}v_z \tag{11}$$

where ν_0 is the hover inflow velocity given by Eq. (9).

Since the aim is to develop a model that is identifiable from experimental data, the values for the positive constants C_{ν_x} and C_{ν_z} will be implicitly chosen to best fit the selected data. An example of this fit for the small quadrotor considered in [28] is illustrated in Figure 3, where the curvy surface defined by Eq. (10) is approximated by the plane defined by Eq. (11).

Defining the *hover inflow ratio* $\mu_0 = \frac{\nu_0}{\Omega R}$ and *vertical advance ratio* $\mu_z = \frac{v_z}{\Omega R}$, the total inflow ratio λ becomes

$$\lambda = \mu_0 - C_{\nu_x}\mu_x - (C_{\nu_z} - 1)\mu_z \tag{12}$$

Let $C_\sigma = \frac{N_\mathrm{b}\bar{c}a}{2\pi R}$, $C_{\theta_1} = \frac{\theta_0}{3} + \frac{\theta_\mathrm{tw}}{4}$, and $C_{\theta_2} = \frac{\theta_0}{2} + \frac{\theta_\mathrm{tw}}{4}$. The rotor coefficients in Eq. (8) are expanded using Eq. (12) to obtain the non-dimensional rotor force coefficients,

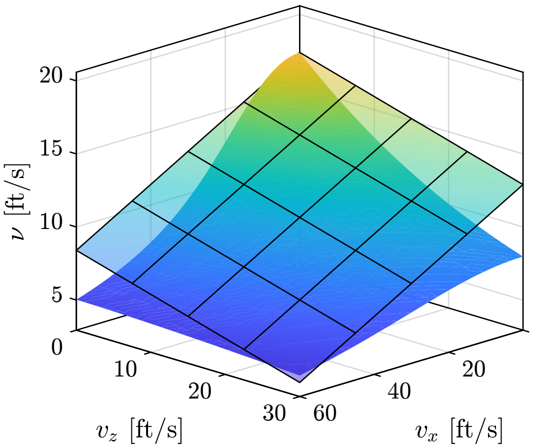

Fig. 3 Steady inflow model (10) **and the linear approximation** (11)**.**

$$\begin{aligned}C_H = &-\underbrace{\tfrac{1}{2a}C_\sigma \bar{c}_d}_{C_{H_{\mu_x}}}\mu_x - \underbrace{C_\sigma C_{\theta_2}}_{C_{H_{\mu_0,\mu_x}}}\mu_x\mu_0 + \underbrace{C_\sigma C_{\theta_2} C_{\nu_x}}_{C_{H_{\mu_x^2}}}\mu_x^2 \\ &+ \underbrace{C_\sigma C_{\theta_2}(C_{\nu_z}-1)}_{C_{H_{\mu_x,\mu_z}}}\mu_x\mu_z\end{aligned} \tag{13a}$$

$$\begin{aligned}C_T = &\underbrace{C_\sigma C_{\theta_1}}_{C_{T_0}} - \underbrace{\tfrac{1}{2}C_\sigma}_{C_{T_{\mu_0}}}\mu_0 + \underbrace{\tfrac{1}{2}C_\sigma C_{\nu_x}}_{C_{T_{\mu_x}}}\mu_x + \underbrace{C_\sigma C_{\theta_2}}_{C_{T_{\mu_x^2}}}\mu_x^2 \\ &+ \underbrace{\tfrac{1}{2}C_\sigma(C_{\nu_z}-1)}_{C_{T_{\mu_z}}}\mu_z\end{aligned} \tag{13b}$$

and moment coefficients,

$$\begin{aligned}C_{\mathcal{R}} = &-\underbrace{C_\sigma C_{\theta_1}}_{C_{R_{\mu_x}}}\mu_x + \underbrace{\tfrac{1}{4}C_\sigma}_{C_{R_{\mu_0,\mu_x}}}\mu_x\mu_0 - \underbrace{\tfrac{1}{4}C_\sigma C_{\nu_x}}_{C_{R_{\mu_x^2}}}\mu_x^2 \\ &- \underbrace{\tfrac{1}{4}C_\sigma(C_{\nu_z}-1)}_{C_{R_{\mu_x,\mu_z}}}\mu_x\mu_z\end{aligned} \tag{13c}$$

$$\begin{aligned}C_{\mathcal{Q}} = &-\underbrace{\tfrac{1}{4a}C_\sigma\bar{c}_d}_{C_{Q_0}} - \underbrace{C_\sigma C_{\theta_1}}_{C_{Q_{\mu_0}}}\mu_0 + \underbrace{C_\sigma C_{\theta_1} C_{\nu_x}}_{C_{Q_{\mu_x}}}\mu_x \\ &+ \underbrace{C_\sigma C_{\theta_1}(C_{\nu_z}-1)}_{C_{Q_{\mu_z}}}\mu_z + \underbrace{\tfrac{1}{2}C_\sigma}_{C_{Q_{\mu_0^2}}}\mu_0^2 - \underbrace{C_\sigma\left(\tfrac{\bar{c}_d}{4a} - \tfrac{C_{\nu_x}^2}{2}\right)}_{C_{Q_{\mu_x^2}}}\mu_x^2 \\ &+ \underbrace{\tfrac{1}{2}C_\sigma(C_{\nu_z}-1)^2}_{C_{Q_{\mu_z^2}}}\mu_z^2 - \underbrace{C_\sigma C_{\nu_x}}_{C_{Q_{\mu_0,\mu_x}}}\mu_0\mu_x \\ &- \underbrace{C_\sigma(C_{\nu_z}-1)}_{C_{Q_{\mu_0,\mu_z}}}\mu_0\mu_z + \underbrace{C_\sigma C_{\nu_x}(C_{\nu_z}-1)}_{C_{Q_{\mu_x,\mu_z}}}\mu_x\mu_z\end{aligned} \tag{13d}$$

Because the ultimate aim is to identify a flight dynamic model from experimental data, constant parameters in Eq. (13) are lumped together to define a new set of parameters which will appear in the final multirotor model. Notice Eq. (13) comprises second-order polynomials of the advance ratios μ_x, μ_z, and μ_0. Hence, we refer to the quadratic terms (e.g., $C_{H_{\mu_x^2}}\mu_x^2$) in the model as *second-order effects*.

Remark 1 *The lumped rotor aerodynamic parameters in Eq.* (13) *are non-dimensional.*

The rotor aerodynamic analysis presented here provides a physically motivated model structure, but specific coefficient values will be determined from data for the complete aircraft, not from computations of the expressions above. Although the set of five base parameters $\{C_\sigma, C_{\nu_x}, C_{\nu_z}, C_{\theta_1}, C_{\theta_2}\}$ could be used in the final model structure, we choose to decouple these interdependent parameters (e.g., $C_{T_0} \neq C_{R_{\mu_x}}$) to better capture unmodeled effects and potential violations of Assumption 2.

For the steadily translating rotor depicted in Figure 2, the isolated body-frame rotor force $\boldsymbol{F}_{\rm r} = [X_{\rm r}\ \ Y_{\rm r}\ \ Z_{\rm r}]^\mathsf{T}$ and moment $\boldsymbol{M}_{\rm r} = [\mathcal{L}_{\rm r}\ \ \mathcal{M}_{\rm r}\ \ \mathcal{N}_{\rm r}]^\mathsf{T}$ applied to the rotor hub satisfy

$$\begin{bmatrix} X_{\rm r} \\ Y_{\rm r} \\ Z_{\rm r}\end{bmatrix} = \begin{bmatrix} H\cos\beta_f \\ -H\sin\beta_f \\ -T\end{bmatrix} \qquad \begin{bmatrix} \mathcal{L}_{\rm r} \\ \mathcal{M}_{\rm r} \\ \mathcal{N}_{\rm r}\end{bmatrix} = \begin{bmatrix} \mathcal{R}\cos\beta_f \\ -\mathcal{R}\sin\beta_f \\ -\mathcal{Q}\end{bmatrix} \tag{14}$$

Using the redimensionalized lumped-parameter expressions (13) along with the velocity component relation in Eq. (2), we have the following isolated rotor model:

$$\begin{aligned}X_{\rm r} = \rho\pi R^2\big(&-C_{H_{\mu_x}}R\Omega u - C_{H_{\mu_0,\mu_x}}\nu_0 u + C_{H_{\mu_x^2}}v_x u \\ &- C_{H_{\mu_x,\mu_z}}uw\big)\end{aligned} \tag{15a}$$

$$\begin{aligned}Y_{\rm r} = \rho\pi R^2\big(&-C_{H_{\mu_x}}R\Omega v - C_{H_{\mu_0,\mu_x}}\nu_0 v + C_{H_{\mu_x^2}}v_x v \\ &- C_{H_{\mu_x,\mu_z}}vw\big)\end{aligned} \tag{15b}$$

$$\begin{aligned}Z_{\rm r} = \rho\pi R^2\big(&-C_{T_0}R^2\Omega^2 + C_{T_{\mu_0}}R\Omega\nu_0 - C_{T_{\mu_x}}R\Omega v_x \\ &+ C_{T_{\mu_z}}R\Omega w - C_{T_{\mu_x^2}}v_x^2\big)\end{aligned} \tag{15c}$$

$$\begin{aligned}\mathcal{L}_{\rm r} = \rho\pi R^3\big(&-C_{R_{\mu_x}}R\Omega u + C_{R_{\mu_0,\mu_x}}\nu_0 u - C_{R_{\mu_x^2}}v_x u \\ &+ C_{R_{\mu_x,\mu_z}}uw\big)\end{aligned} \tag{15d}$$

$$\begin{aligned}\mathcal{M}_{\rm r} = \rho\pi R^3\big(&-C_{R_{\mu_x}}R\Omega v + C_{R_{\mu_0,\mu_x}}\nu_0 v - C_{R_{\mu_x^2}}v_x v \\ &+ C_{R_{\mu_x,\mu_z}}vw\big)\end{aligned} \tag{15e}$$

$$\begin{aligned}\mathcal{N}_{\rm r} = \rho\pi R^3\big(&C_{Q_0}R^2\Omega^2 + C_{Q_{\mu_0}}R\Omega\nu_0 - C_{Q_{\mu_x}}R\Omega v_x \\ &+ C_{Q_{\mu_z}}R\Omega w - C_{Q_{\mu_0^2}}\nu_0^2 - C_{Q_{\mu_x^2}}v_x^2 - C_{Q_{\mu_z^2}}w^2 \\ &+ C_{Q_{\mu_0,\mu_x}}\nu_0 v_x - C_{Q_{\mu_0,\mu_z}}\nu_0 w + C_{Q_{\mu_x,\mu_z}}v_x w\big)\end{aligned} \tag{15f}$$

Equation (15) gives the components of the force and moment vectors, expressed in the body frame, applied to the hub of an isolated rotor that is steadily translating in still air. This model is adopted for the rotor aerodynamics of the multirotor aircraft considered in Section III, where we consider the effects of multiple rotors arranged in a regular pattern about the $\boldsymbol{b}_3$-axis of a translating and rotating body frame.

III. Multirotor Forces and Moments

The rotor aerodynamic force and moment described in Eq. (15) are incomplete representations of the actual force and moment applied to the airframe. Here, we consider several additional factors that influence a given rotor's effect on vehicle motion.

A. Motor Dynamics

Consider a motor fixed in space that is attached to the rotor depicted in Figure 2. Although there are many approaches to electric propulsion of multirotor aircraft, we consider the common assumption (also adopted by Cunningham and Hubbard [11], Khan and Nahon [29], for example) that the system comprising the motor and electronic speed controller (ESC) is well-described by the DC motor model

$$L_{\mathrm{m}}\frac{\mathrm{d}i_{\mathrm{m}}}{\mathrm{d}t}+R_{\mathrm{m}}i_{\mathrm{m}}+k_{\mathrm{v}}\Omega=v_{\mathrm{m}} \tag{16a}$$

$$J_z\frac{\mathrm{d}\Omega}{\mathrm{d}t}=\mathcal{Q}_{\mathrm{m}}+\mathcal{Q} \tag{16b}$$

where L_{m} is the armature inductance, i_{m} is the armature current, R_{m} is the armature resistance, k_{v} is the back electro-magnetic force constant (often called the velocity constant), v_{m} is the voltage supplied to the motor, J_z is the moment of inertia of the motor and rotor rigid body about the $\boldsymbol{r}_3$ axis, $\mathcal{Q}_{\mathrm{m}}$ is the torque applied to the rotor about its spin axis by the motor mounted to the airframe (a function of i_{m} and Ω), and $\mathcal{Q}$ is the aerodynamic torque acting on the rotor about its spin axis. The motor model in Eq. (16) may be simplified through use of the torque constant, k_{t}, which is a proportional constant relating $\mathcal{Q}_{\mathrm{m}}$ to i_{m}. Furthermore, the motor/ESC electrical dynamics evolve on a much faster time scale than the mechanical motor speed dynamics so that the steady-state solution to Eq. (16a) may be used to obtain

$$J_z\dot{\Omega}=-\frac{k_{\mathrm{t}}k_{\mathrm{v}}}{R_{\mathrm{m}}}\Omega+\frac{k_{\mathrm{t}}}{R_{\mathrm{m}}}v_{\mathrm{m}}+\mathcal{Q} \tag{17}$$

as corroborated by [11].

Similar to [2], we recognize that the motor dynamics influence the rigid body in three dimensions. Consider the ith motor located at the point $\boldsymbol{p}_i=[x_i\ \ y_i\ \ z_i]^{\mathsf{T}}$ in the body frame. Let $\boldsymbol{\Omega}_i=[0\ 0\ \sigma_i\Omega_i]^{\mathsf{T}}$ be its angular velocity vector with respect to the body frame, expressed in the body frame, where $\sigma_i\in\{-1,+1\}$ represents the rotor rotation direction according to the right-hand rule in the body frame. Assuming the motor inertia J_z is much smaller than the rigid-body moment of inertia about the $\boldsymbol{b}_3$ axis and that the magnitude of the yaw rate is much less than the motor speed,

$$\boldsymbol{J}\dot{\boldsymbol{\Omega}}_i=\boldsymbol{J}\boldsymbol{\Omega}_i\times\boldsymbol{\omega}-\boldsymbol{M}_{\mathrm{m},i}+\boldsymbol{M}_{\mathrm{r},i} \tag{18}$$

where $\boldsymbol{J}=\mathbf{diag}(J_x,J_y,J_z)$ is the moment of inertia matrix of the motor/rotor rigid body, $\boldsymbol{M}_{\mathrm{m},i}$ is the moment applied to the airframe (hence the sign reversal compared to Eq. (16b)), and

$$\boldsymbol{M}_{\mathrm{r},i}=-\sigma_i\begin{bmatrix}\mathcal{L}_{\mathrm{r},i}\\ \mathcal{M}_{\mathrm{r},i}\\ \mathcal{N}_{\mathrm{r},i}\end{bmatrix} \tag{19}$$

is the aerodynamic moment on the ith rotor expressed in the body frame. Equation (18) constitutes one dynamical equation for the rotor spin rate — the third component of $\boldsymbol{\Omega}_i$ — and two algebraic equations for the moments exerted by the motor on the airframe about the non-spin axes — the first and second components of $\boldsymbol{M}_{\mathrm{m},i}$. Here, as opposed to the isolated rotor moment components in Eq. (15), the rotor aerodynamic moments are evaluated at the velocities of the rotor hubs, $\boldsymbol{v}_i$, accounting for the body angular velocity $\boldsymbol{\omega}$. As in [17], we assume knowledge of $\dot{\Omega}_i$ so that an expression for $\boldsymbol{M}_{\mathrm{m},i}$ in terms of motor parameters and/or electrical states is not needed. Instead, we rearrange and simplify Eq. (18) to obtain the moment applied to the airframe by a single rotor,

$$\boldsymbol{M}_{\mathrm{m},i}=\boldsymbol{M}_{\mathrm{r},i}-\sigma_iJ_z\begin{bmatrix}q\Omega_i\\ -p\Omega_i\\ \dot{\Omega}_i\end{bmatrix} \tag{20}$$

Equation (20) shows the relationship between the rotor aerodynamic moments derived in Section II and the moment applied to the rigid airframe by a single rotor. The terms $J_zq\Omega_i$ and $J_zp\Omega_i$ are the gyroscopic effects of the motor/rotor, and $J_z\dot{\Omega}_i$ is net motor torque. The transmission of rotor aerodynamic forces is much simpler than that of the moments. The aerodynamic force of the ith rotor applied to the airframe at the base of the motor is

$$\boldsymbol{F}_{\mathrm{m},i}=\boldsymbol{F}_{\mathrm{r},i} \tag{21}$$

whose components are given by Eqs. (15a)–(15c), evaluated using the local rotor hub velocity, $\boldsymbol{v}_i$. Equations (21) and (20) define the force and moment, respectively, applied by the ith motor to the rigid airframe at its point of attachment.

B. Multirotor Aerodynamics

With an understanding of how forces and moments are transmitted to the airframe from Section III.A, and the individual rotor force and moment expressions developed in Section II, we can derive expressions for the total force and moment on a multirotor aircraft. Let the total force and moment applied to the airframe be $\boldsymbol{F}=[F_x\ \ F_y\ \ F_z]^{\mathsf{T}}$ and $\boldsymbol{M}=[M_x\ \ M_y\ \ M_z]^{\mathsf{T}}$, respectively. Consider a multirotor aircraft whose configuration is defined by the following assumptions.

Assumption 4

a) *The number of rotors,* $N_{\mathrm{r}}\geq 4$*, is even.*
b) *The rotors counter-rotate in an alternating fashion (i.e., neighboring rotors spin in opposite directions).*
c) *The rotor configuration is symmetric about the* $\boldsymbol{b}_1$ *and* $\boldsymbol{b}_2$ *axes.*
d) *The rotor arms have equal length,* ℓ*, and are arranged with equal interior angles,* $2\pi/N_{\mathrm{r}}$*.*
e) *The rotors are uncanted (coplanar) and located at the same height,* $h=-z_i$*, above the center of gravity.*

As an example, a quadrotor in a symmetric "X" configuration as pictured in Figure 4 satisfies Assumption 4.

As it will be important for the final model, we define three classes of configurations that satisfy Assumption 4.

Definition 1

a) *A* quadrotor$_{+}$ *satisfies Assumption 4 with* $N_{\mathrm{r}}=4$ *and* $(x_i,y_i)=(0,\ell)$ *for some* $i\in\{1,2,3,4\}$.
b) *A* quadrotor$_{\times}$ *satisfies Assumption 4 with* $N_{\mathrm{r}}=4$ *and* $(x_i,y_i)=(\ell\frac{\sqrt{2}}{2},\ell\frac{\sqrt{2}}{2})$ *for some* $i\in\{1,2,3,4\}$.
c) *A* multirotor$_{\geq 6}$ *satisfies Assumption 4 for* $N_{\mathrm{r}}\geq 6$.

Remark 2 *Although the following derivation considers the configuration in Assumption 4, the same approach may be used for any other configuration of interest.*

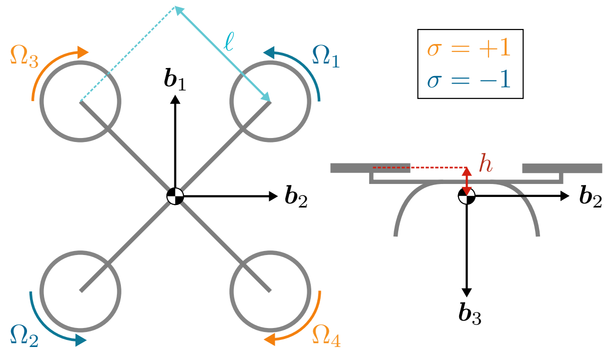

Fig. 4 Quadrotor geometry

There is no established convention for modeling the aerodynamics of a multirotor airframe with the rotors removed. Geometries and their aerodynamic characteristics vary widely. For this reason, experimentally-derived [30, 31] and/or simplified-geometry models [32, 33] are considered. We assume the following.

Assumption 5 *The airframe aerodynamic force and moment are well-approximated by empirically-derived expressions that depend on body-frame translational and angular velocity.*

In reality, the flow induced by the rotors interacts with the airframe as well as among the rotors themselves. These complicated interactions [8] are the dominant aerodynamic effect of the airframe, and they are not captured by superposing a bare airframe aerodynamic model. For this reason, we make the following assumption.

Assumption 6 *The force and moment due to rotor-airframe and rotor-rotor interaction are captured within the aggregate airframe and rotor force and moment models.*

As a consequence of Assumption 6, any rotor aerodynamic interactions will be expressed in the model as either a decrease in thrust or an increase in rotor and airframe drag (in the steady state, at least). Any unsteady effects of aerodynamic interactions are not captured by the model.

Because the motors are assumed to be rigidly attached to the aircraft, the body frame force, $\boldsymbol{F}$, is equal to the total rotor aerodynamic force, $\boldsymbol{F}_\mathrm{r} = [X_\mathrm{r} \;\; Y_\mathrm{r} \;\; Z_\mathrm{r}]^\mathsf{T}$, plus the airframe aerodynamic force, $\boldsymbol{F}_\mathrm{a} = [X_\mathrm{a} \;\; Y_\mathrm{a} \;\; Z_\mathrm{a}]^\mathsf{T}$. Here, $\boldsymbol{F}_\mathrm{r}$ and $\boldsymbol{M}_\mathrm{r}$ denote the total rotor-derived force and moment vectors applied to the aircraft as opposed to the isolated rotor force/moment components considered in Eq. (15). Thus, we have

$$\boldsymbol{F} = \boldsymbol{F}_\mathrm{r} + \boldsymbol{F}_\mathrm{a} = \sum_{i=1}^{N_\mathrm{r}} \boldsymbol{F}_{\mathrm{r},i} + \boldsymbol{F}_\mathrm{a} = \sum_{i=1}^{N_\mathrm{r}} \boldsymbol{F}_{\mathrm{m},i} + \boldsymbol{F}_\mathrm{a} \tag{22}$$

As shown in Section III.A, however, $\boldsymbol{M}$ is not simply the sum of the airframe aerodynamic moment, $\boldsymbol{M}_\mathrm{a} = [\mathcal{L}_\mathrm{a} \;\; \mathcal{M}_\mathrm{a} \;\; \mathcal{N}_\mathrm{a}]^\mathsf{T}$, and the total rotor aerodynamic moment,

$$\boldsymbol{M}_\mathrm{r} = \sum_{i=1}^{N_\mathrm{r}} (\boldsymbol{M}_{\mathrm{r},i} + \boldsymbol{p}_i \times \boldsymbol{F}_{\mathrm{r},i}) =: \begin{bmatrix} \mathcal{L}_\mathrm{r} \\ \mathcal{M}_\mathrm{r} \\ \mathcal{N}_\mathrm{r} \end{bmatrix} \tag{23}$$

Instead, referring to Eqs. (20) and (21),

$$\boldsymbol{M} = \sum_{i=1}^{N_\mathrm{r}} (\boldsymbol{M}_{\mathrm{m},i} + \boldsymbol{p}_i \times \boldsymbol{F}_{\mathrm{m},i}) + \boldsymbol{M}_\mathrm{a} \tag{24}$$

Alternatively, the total applied moment in Eq. (24) can be written using the total aerodynamic moment in Eq. (23) as

$$\boldsymbol{M} = \boldsymbol{M}_\mathrm{r} + \boldsymbol{M}_\mathrm{a} - J_z \sum_{i=1}^{N_\mathrm{r}} \sigma_i \begin{bmatrix} q\Omega_i \\ -p\Omega_i \\ \dot{\Omega}_i \end{bmatrix} \tag{25}$$

Furthermore, we must determine for each rotor the contribution of vehicle angular velocity to the rotor aerodynamic force and moment. These forces and moments are defined in the body frame whose origin does not coincide with the rotor hubs. Recalling from Assumption 4 that the rotors are not canted, i.e., the $\boldsymbol{r}_1$-$\boldsymbol{r}_2$ plane is parallel to the $\boldsymbol{b}_1$-$\boldsymbol{b}_2$ plane, the local velocity of the ith rotor hub in the body frame is

$$\boldsymbol{v}_i = \boldsymbol{v} + \boldsymbol{\omega} \times \boldsymbol{p}_i \tag{26}$$

Incorporating this correction yields a complicated model structure, making parameter estimation from flight data difficult. To obtain a more compact and identifiable form, we make the following assumption.

Assumption 7 *When computing the local velocity for each rotor, the vehicle yaw rate, r, and the vertical moment arm, h, can be neglected.*

Assumption 7 reflects the expectation that the primary contribution of the vehicle angular velocity to the rotor forces and moments is the resulting change in inflow velocity. Following Assumption 7, we approximate the local velocity of the ith rotor as

$$\boldsymbol{v}_i \approx \boldsymbol{v} + \begin{bmatrix} p \\ q \\ 0 \end{bmatrix} \times \begin{bmatrix} x_i \\ y_i \\ 0 \end{bmatrix} = \begin{bmatrix} u \\ v \\ w + py_i - qx_i \end{bmatrix} \tag{27}$$

Given the local rotor velocity approximation in Eq. (27), the next step is to express the total force and moment in a form that simplifies control, analysis, and the design of excitation signals for system identification. Rather than using individual rotor speeds as inputs, which can be cumbersome and hard to interpret, we define a more compact representation using *virtual actuators*, which are defined by the *motor mixing* formula

$$\underbrace{\begin{bmatrix} \delta^2 t \\ \delta^2 a \\ \delta^2 e \\ \delta^2 r \end{bmatrix}}_{\boldsymbol{\delta}^2} := \mathbf{M_{ix}} \underbrace{\begin{bmatrix} \Omega_1^2 \\ \Omega_2^2 \\ \vdots \\ \Omega_{N_\mathrm{r}}^2 \end{bmatrix}}_{\boldsymbol{\Omega}^2} \tag{28}$$

where $\mathbf{M_{ix}}$ is determined by the geometry of the aircraft as follows:

$$\mathbf{M_{ix}} = \begin{bmatrix} 1/N_\mathrm{r} & 1/N_\mathrm{r} & \cdots & 1/N_\mathrm{r} \\ -y_1 & -y_2 & \cdots & -y_{N_\mathrm{r}} \\ x_1 & x_2 & \cdots & x_{N_\mathrm{r}} \\ -\sigma_1 & -\sigma_2 & \cdots & -\sigma_{N_\mathrm{r}} \end{bmatrix} \tag{29}$$

To capture first-order rotor speed terms, we also define

$$\underbrace{\begin{bmatrix} \delta t \\ \delta a \\ \delta e \\ \delta r \end{bmatrix}}_{\boldsymbol{\delta}} := \mathbf{M_{ix}} \underbrace{\begin{bmatrix} \Omega_1 \\ \Omega_2 \\ \vdots \\ \Omega_{N_\mathrm{r}} \end{bmatrix}}_{\boldsymbol{\Omega}} \tag{30}$$

In Eqs. (28) and (30), $\boldsymbol{\delta}^2$ and $\boldsymbol{\delta}$ serve as virtual actuators, providing a more compact representation of control inputs; $\boldsymbol{\Omega}^2$ and $\boldsymbol{\Omega}$ are the column vectors of squared and positive motor speeds, respectively. Specifically, δa, δe, δr, and δt represent virtual aileron, elevator, rudder, and thrust inputs. However, it is important to note that $\boldsymbol{\delta}^2$ and $\boldsymbol{\delta}$ are not independently controlled.

Finally, the body frame forces and moments are obtained using Eqs. (22) and (25), where $\boldsymbol{F}_{\mathrm{r},i}$ and $\boldsymbol{M}_{\mathrm{r},i}$ are evaluated using the hub velocity $\boldsymbol{v}_i$ as defined in Eq. (27) and rotor speeds are replaced using the virtual actuator definitions in Eqs. (28) and (30). As a result, we obtain the following model.

Model 1 *The force and moment components for a multirotor aircraft satisfying Assumption 4 are*

$$\begin{aligned} F_x = \rho\pi R^2 N_\mathrm{r} u \Big(&-C_{H_{\mu_x}} R\delta t - C_{H_{\mu_0,\mu_x}} \nu_0 + C_{H_{\mu_x^2}} v_x \\ &- C_{H_{\mu_x,\mu_z}} w \Big) + X_\mathrm{a} \end{aligned} \tag{31a}$$

$$\begin{aligned} F_y = \rho\pi R^2 N_\mathrm{r} v \Big(&-C_{H_{\mu_x}} R\delta t - C_{H_{\mu_0,\mu_x}} \nu_0 + C_{H_{\mu_x^2}} v_x \\ &- C_{H_{\mu_x,\mu_z}} w \Big) + Y_\mathrm{a} \end{aligned} \tag{31b}$$

$$\begin{aligned} F_z = \rho\pi R^2 \Big(&-C_{T_0} R^2 N_\mathrm{r} \delta^2 t + C_{T_{\mu_0}} R N_\mathrm{r} \nu_0 \delta t \\ &- C_{T_{\mu_x}} R N_\mathrm{r} v_x \delta t + C_{T_{\mu_z}} R (N_\mathrm{r} w \delta t - \Delta\nu_Z) \\ &- C_{T_{\mu_x^2}} N_\mathrm{r} v_x^2 \Big) + Z_\mathrm{a} \end{aligned} \tag{31c}$$

$$\begin{aligned} M_x = \rho\pi R^2 \Big(&-C_{R_{\mu_x}} R^2 u \delta r + C_{T_0} R^2 \delta^2 a - C_{T_{\mu_0}} R \nu_0 \delta a \\ &+ C_{T_{\mu_x}} R v_x \delta a - C_{T_{\mu_z}} R \big(w\delta a - \Delta\nu_{\mathcal{L}} \big) \\ &- C_{H_{\mu_x}} R N_\mathrm{r} h v \delta t - C_{H_{\mu_0,\mu_x}} N_\mathrm{r} h v \nu_0 \\ &+ C_{H_{\mu_x^2}} N_\mathrm{r} h v v_x - C_{H_{\mu_x,\mu_z}} N_\mathrm{r} h v w \Big) \\ &+ \mathcal{L}_\mathrm{a} + J_z q \delta r \end{aligned} \tag{31d}$$

$$\begin{aligned} M_y = \rho\pi R^2 \Big(&-C_{R_{\mu_x}} R^2 v \delta r + C_{T_0} R^2 \delta^2 e - C_{T_{\mu_0}} R \nu_0 \delta e \\ &+ C_{T_{\mu_x}} R v_x \delta e - C_{T_{\mu_z}} R \big(w\delta e - \Delta\nu_{\mathcal{M}} \big) \\ &+ C_{H_{\mu_x}} R N_\mathrm{r} h u \delta t + C_{H_{\mu_0,\mu_x}} N_\mathrm{r} h u \nu_0 \\ &- C_{H_{\mu_x^2}} N_\mathrm{r} h u v_x + C_{H_{\mu_x,\mu_z}} N_\mathrm{r} h u w \Big) \\ &+ \mathcal{M}_\mathrm{a} - J_z p \delta r \end{aligned} \tag{31e}$$

$$\begin{aligned} M_z = \rho\pi R^2 \Big(&C_{Q_0} R^3 \delta^2 r + C_{Q_{\mu_0}} R^2 \nu_0 \delta r - C_{Q_{\mu_x}} R^2 v_x \delta r \\ &+ C_{Q_{\mu_z}} R^2 \big(w\delta r - \Delta\nu_{\mathcal{N}} \big) - C_{Q_{\mu_z^2}} R \Delta\nu_{\mathcal{N}}^2 \\ &- C_{H_{\mu_x}} R (u\delta a + v\delta e) + \tfrac{1}{2} C_{H_{\mu_x,\mu_z}} N_\mathrm{r} \ell^2 (up + vq) \Big) \\ &+ \mathcal{N}_\mathrm{a} + J_z \dot{\delta r} \end{aligned} \tag{31f}$$

where $\Delta\nu_Z = p\delta a + q\delta e$ *and*

$$\Delta\nu_{\mathcal{L}} = \begin{cases} \frac{1}{2}\ell^2 p (N_\mathrm{r}\delta t + \delta r) & \text{quadrotor}_+ \\ \frac{1}{2}\ell^2 (N_\mathrm{r} p \delta t + q\delta r) & \text{quadrotor}_\times \\ \frac{1}{2}\ell^2 N_\mathrm{r} p \delta t & \text{multirotor}_{\geq 6} \end{cases}$$

$$\Delta\nu_{\mathcal{M}} = \begin{cases} \frac{1}{2}\ell^2 q (N_\mathrm{r}\delta t - \delta r) & \text{quadrotor}_+ \\ \frac{1}{2}\ell^2 (N_\mathrm{r} q \delta t + p\delta r) & \text{quadrotor}_\times \\ \frac{1}{2}\ell^2 N_\mathrm{r} q \delta t & \text{multirotor}_{\geq 6} \end{cases}$$

$$\Delta\nu_{\mathcal{N}} = \begin{cases} p\delta a - q\delta e & \text{quadrotor}_+ \\ p\delta e + q\delta a & \text{quadrotor}_\times \\ 0 & \text{multirotor}_{\geq 6} \end{cases}$$

$$\Delta\nu_{\mathcal{N}}^2 = \begin{cases} \frac{1}{2} N_\mathrm{r} \ell^2 (p^2 - q^2) & \text{quadrotor}_+ \\ N_\mathrm{r} \ell^2 pq & \text{quadrotor}_\times \\ 0 & \text{multirotor}_{\geq 6} \end{cases}$$

A detailed derivation of Model 1 is given in the Appendix. Note the configuration-dependent terms, $\Delta\nu_{(\cdot)}$, stem from the effect of angular velocity on the change in total rotor inflow.

Remark 3 *The terms in Model 1 that do not explicitly depend on rotor speed retain implicit dependence through the induced inflow velocity model in Eq.* (11)*. By choosing a linear inflow model, we have replaced the physically meaningful structure of Eq.* (10) *with an experimentally determined approximation* (11)*. The constant parameters* $C_{H_{\mu_0,\mu_x}}$, $C_{H_{\mu_x^2}}$, $C_{H_{\mu_x,\mu_z}}$, *and* $C_{Q_{\mu_z^2}}$ *implicitly depend on the aggregate rotor speed data used to identify their values. The only exception is* $C_{T_{\mu_x^2}}$ *term, which does not arise from the inflow model.*

This proposed model has several benefits when used for control and estimation. Mainly, this model structure is valid over a large range of velocities. For steady flight in any direction, except for descending flight into a vortex ring state [34], there are few approximations made in progressing from the initial blade element theory to the final model. The model remains valid under large roll and pitch rate perturbations from translating flight because the local rotor velocity is incorporated directly. Furthermore, the use of virtual actuators instead of rotor speeds not only generalizes the model to any configuration satisfying Assumption 4, but also reveals an intuitive understanding of non-trivial effects such as $C_{H_{\mu_x}} R(u\delta a + v\delta e)$ in the yawing moment equation, M_z. This term captures the yawing moment due to differential drag under virtual aileron and elevator commands; it is similar to adverse/proverse yaw for a fixed-wing aircraft.

However, Model 1 ignores effects that might be important in some applications. First, the angular velocity of the aircraft is not considered in the blade-element forces and moments beyond its effect on the rotor hub velocity. In applications where the vehicle is rapidly rotating (e.g., upset recovery from tumbling motion), incorporating angular velocity in the blade-element loads may be beneficial. Second, general blade motion, inflow dynamics, and other unsteady effects are neglected. While the linear approximation in Eq. (11) is not a bad approximation of the steady inflow condition, time-varying inflow effects may be important to model when controlling or estimating motion at fast time scales.

C. Incorporation of Motor Dynamics

When used for state and/or disturbance estimation, the virtual actuators can be treated as inputs or may be estimated as states. In control applications, however, one must acknowledge that the virtual actuators $\boldsymbol{\delta}$ and $\boldsymbol{\delta}^2$ are not independently controlled. To resolve this issue, $\boldsymbol{\delta}$ and $\boldsymbol{\delta}^2$ may be included in a motor model, such as Eq. (17), whose input corresponds to physically realizable motor commands. In vector form, where $\boldsymbol{\mathcal{Q}} = [\mathcal{Q}_1 \cdots \mathcal{Q}_{N_\mathrm{r}}]^\mathsf{T}$ and $\boldsymbol{v}_\mathrm{m} = [v_{\mathrm{m},1} \cdots v_{\mathrm{m},N_\mathrm{r}}]^\mathsf{T}$, Eq. (17) becomes

$$J_z \dot{\boldsymbol{\Omega}} = -\frac{k_\mathrm{t} k_\mathrm{v}}{R_\mathrm{m}} \boldsymbol{\Omega} + \frac{k_\mathrm{t}}{R_\mathrm{m}} \boldsymbol{v}_\mathrm{m} + \boldsymbol{\mathcal{Q}} \tag{32}$$

Pre-multiplying both sides by $\mathbf{M_{ix}}$ and defining the actuator control input

$$\boldsymbol{u}_\delta \coloneqq \frac{1}{k_\mathrm{v}} \mathbf{M_{ix}} \boldsymbol{v}_\mathrm{m} \tag{33}$$

we obtain

$$J_z \dot{\boldsymbol{\delta}} = -\frac{k_\mathrm{t} k_\mathrm{v}}{R_\mathrm{m}} \boldsymbol{\delta} + \frac{k_\mathrm{t} k_\mathrm{v}}{R_\mathrm{m}} \boldsymbol{u}_\delta + \mathbf{M_{ix}} \boldsymbol{\mathcal{Q}} \tag{34}$$

Unlike in the derivation of the yawing moment equation (31f), the second-order rotor torque coefficients, such as $C_{Q_{\mu_x^2}}$ and $C_{Q_{\mu_0,\mu_x}}$, do not completely vanish from the term $\mathbf{M_{ix}}\boldsymbol{\mathcal{Q}}$ in Eq. (34). This introduces complexity into the model, with many terms that have negligible influence. To simplify the actuator model, we neglect these second-order torque coefficients (as defined in Eq.(13d)) to yield

$$\begin{aligned} J_z \dot{\boldsymbol{\delta}} = &-\frac{k_\mathrm{t} k_\mathrm{v}}{R_\mathrm{m}} \boldsymbol{\delta} + \frac{k_\mathrm{t} k_\mathrm{v}}{R_\mathrm{m}} \boldsymbol{u}_\delta + \rho \pi R^3 \Big(C_{Q_0} R^2 \boldsymbol{\delta}^2 \\ &+ C_{Q_{\mu_0}} R \nu_0 \boldsymbol{\delta} + C_{Q_{\mu_x}} R v_x \boldsymbol{\delta} - C_{Q_{\mu_z}} R \left(w \boldsymbol{\delta} - \boldsymbol{\Delta} \right) \Big) \end{aligned} \tag{35}$$

where $\boldsymbol{\Delta} = [\Delta\nu_Z/N_\mathrm{r} \;\; \Delta\nu_\mathcal{L} \;\; \Delta\nu_\mathcal{M} \;\; \Delta\nu_\mathcal{N}]^\mathsf{T}$.

Remark 4 *It is important to note that these second-order coefficients do vanish in the virtual rudder dynamics (the final component of Eq.* (34)*). As a result, the simplified actuator dynamics*(35) *remain consistent with the yawing moment equation* (31f).

With the primary rotor aerodynamic torques incorporated into the actuator dynamics, we can construct the rigid-body yawing moment, M_z, by substituting the applied motor torque $\boldsymbol{\mathcal{Q}}_\mathrm{m}$ into Eq. (24) to obtain

$$\begin{aligned} M_z = &\frac{k_\mathrm{t} k_\mathrm{v}}{R_\mathrm{m}} \left(\delta r - u_{\delta r} \right) + \rho \pi R^2 \Big(-C_{H_{\mu_x}} R (u \delta a + v \delta e) \\ &+ \tfrac{1}{2} C_{H_{\mu_x,\mu_z}} N_\mathrm{r} \ell^2 (up + vq) \Big) + \mathcal{N}_\mathrm{a} \end{aligned} \tag{36}$$

Note that incorporating a motor model changes where rotor aerodynamic torques $\mathcal{Q}_i$ enter the flight dynamic model. Instead of directly affecting the rigid-body moment M_z, they enter in the actuator dynamics.

D. Nonlinear Model Simplifications

Model 1 captures key multirotor flight physics while facilitating model identification for model-based control design, state and parameter estimation, and simulation. However, the model's complexity may still be impractical for some applications. Here, we consider two optional assumptions, each of which progressively simplifies the model structure. One potential simplification of Model 1 is to neglect the change in induced inflow velocity due to changes in vehicle velocity.

Assumption 8 (Optional) *The induced inflow velocity is constant and equal to the hover inflow velocity ν_0 given by Eq.* (9)*.*

Under Assumption 8, Model 1 simplifies as follows.

Model 2 *The force and moment components for a multirotor aircraft additionally satisfying Assumption 8 are*

$$F_x = \rho \pi R^2 N_\mathrm{r} u \left(-C_{H_{\mu_x}} R \delta t - C_{H_{\mu_0,\mu_x}} \nu_0 - C_{H_{\mu_x,\mu_z}} w \right) + X_\mathrm{a} \tag{37a}$$

$$F_y = \rho \pi R^2 N_\mathrm{r} v \left(-C_{H_{\mu_x}} R \delta t - C_{H_{\mu_0,\mu_x}} \nu_0 - C_{H_{\mu_x,\mu_z}} w \right) + Y_\mathrm{a} \tag{37b}$$

$$\begin{aligned} F_z = \rho \pi R^2 \Big(&-C_{T_0} R^2 N_\mathrm{r} \delta^2 t + C_{T_{\mu_0}} R N_\mathrm{r} \nu_0 \delta t \\ &+ C_{T_{\mu_z}} R (N_\mathrm{r} w \delta t - \Delta\nu_Z) - C_{T_{\mu_x^2}} N_\mathrm{r} v_x^2 \Big) + Z_\mathrm{a} \end{aligned} \tag{37c}$$

$$\begin{aligned} M_x = \rho \pi R^2 \Big(&-C_{R_{\mu_x}} R^2 u \delta r + C_{T_0} R^2 \delta^2 a - C_{T_{\mu_0}} R \nu_0 \delta a \\ &- C_{T_{\mu_z}} R \big(w \delta a - \Delta\nu_\mathcal{L} \big) - C_{H_{\mu_x}} R N_\mathrm{r} h v \delta t \\ &- C_{H_{\mu_0,\mu_x}} N_\mathrm{r} h v \nu_0 - C_{H_{\mu_x,\mu_z}} N_\mathrm{r} h v w \Big) \\ &+ \mathcal{L}_\mathrm{a} + J_z q \delta r \end{aligned} \tag{37d}$$

$$\begin{aligned} M_y = \rho \pi R^2 \Big(&-C_{R_{\mu_x}} R^2 v \delta r + C_{T_0} R^2 \delta^2 e - C_{T_{\mu_0}} R \nu_0 \delta e \\ &- C_{T_{\mu_z}} R \big(w \delta e - \Delta\nu_\mathcal{M} \big) + C_{H_{\mu_x}} R N_\mathrm{r} h u \delta t \\ &+ C_{H_{\mu_0,\mu_x}} N_\mathrm{r} h u \nu_0 + C_{H_{\mu_x,\mu_z}} N_\mathrm{r} h u w \Big) \\ &+ \mathcal{M}_\mathrm{a} - J_z p \delta r \end{aligned} \tag{37e}$$

$$\begin{aligned} M_z = \rho \pi R^2 \Big(&C_{Q_0} R^3 \delta^2 r + C_{Q_{\mu_0}} R^2 \nu_0 \delta r \\ &+ C_{Q_{\mu_z}} R^2 \big(w \delta r - \Delta\nu_\mathcal{N} \big) - C_{Q_{\mu_z^2}} R \Delta\nu_\mathcal{N}^2 \\ &- C_{H_{\mu_x}} R (u \delta a + v \delta e) + \frac{1}{2} C_{H_{\mu_x,\mu_z}} N_\mathrm{r} \ell^2 (up + vq) \Big) \\ &+ \mathcal{N}_\mathrm{a} + J_z \dot{\delta r} \end{aligned} \tag{37f}$$

By assuming the inflow velocity to be the same as in hover, we have lessened the model's utility at high speeds. However, the model structure that remains now smoothly depends on the vehicle velocity, allowing for more flexibility in control law and estimator design. More specifically, Assumption 8 eliminates terms in Model 1 that depend linearly on rotor-plane airspeed, v_x, whose derivative does not exist at $\boldsymbol{v} = \mathbf{0}$. The quadratic term $C_{T_{\mu_x^2}} N_\mathrm{r} v_x^2$ remains in the F_z equation, however, as it does not arise from the assumed inflow model. Practically, this term can be interpreted as an “airspeed-dependent bias" to the thrust model.

Depending on the airframe design, it may be unnecessary to separately model rotor and airframe effects. For many vehicles, the airframe force and moment are small compared to the rotor-based force and moment. Thus, it is often sufficient to lump these terms together to further simplify the Model 2.

Assumption 9 (Optional) *Airframe aerodynamics can be lumped into the rotor aerodynamics.*

Model 3 *The force and moment components for a multirotor aircraft additionally satisfying Assumption 9 are obtained by setting X_a, Y_a, Z_a, $\mathcal{L}_\mathrm{a}$, $\mathcal{M}_\mathrm{a}$, $\mathcal{N}_\mathrm{a}$ to zero in Model 2.*

Model 3 may also be obtained by way of a second-order Taylor series approximation of Model 2 about hover. For some nonlinear control and estimation applications, especially where a Lyapunov stability approach is used [35, Ch. 4], this quadratic structure makes the control and stability problem more tractable.

IV. Multirotor Simulation Experiment

A simulation study was conducted using a high-fidelity multirotor simulation [23] as the "true" dynamics to investigate the utility of the proposed multirotor model. The simulated vehicle is a small, commercial off-the-shelf quadrotor with 14-inch, fixed-pitch rotors. The rigid body forces and moments computed in the simulation were obtained from isolated rotor and airframe wind tunnel data [28]. Thus, one may directly query the simulation's aerodynamics database at given vehicle state and control values in a similar manner to wind tunnel testing and computational aerodynamic prediction techniques. For this analysis, only Model 3 was considered, which was done for two reasons. First, the regressors of Model 1 were highly collinear for the queried data, which made accurate parameter estimation problematic. Second, since the empirically-derived form of airframe aerodynamics can vary substantially among aircraft and flight regimes, we chose to identify and analyze only rotor-derived terms using data for which the airframe force and moment are set to zero.

The test matrix was designed using design of experiments (DOE) and response surface methodology (RSM) techniques [24, 25] to facilitate accurate identification of the terms included in the postulated multirotor model structure. The test factors directly specified in the experiment included body-frame translational velocity (u, v, w), body angular rates (p, q, and r), and rotor speeds (Ω_1, Ω_2, Ω_3, Ω_4). Table 1 lists the model terms associated with the model structure where all constant parameters are combined into coefficients for each of these regressors to estimate model parameters using least-squares regression.

Table 1 Rotor aerodynamics regressors corresponding to Model 3.

Response	Postulated Regressors
X_r	u, uw, $u\Omega_k$
Y_r	v, vw, $v\Omega_k$
Z_r	Ω_k, $w\Omega_k$, $p\Omega_k$, $q\Omega_k$, u^2, v^2, Ω_k^2
$\mathcal{L}_\mathrm{r}$	v, vw, Ω_k, $u\Omega_k$, $v\Omega_k$, $w\Omega_k$, $p\Omega_k$, Ω_k^2, $(q\Omega_k)$
$\mathcal{M}_\mathrm{r}$	u, uw, Ω_k, $u\Omega_k$, $v\Omega_k$, $w\Omega_k$, $q\Omega_k$, Ω_k^2, $(p\Omega_k)$
$\mathcal{N}_\mathrm{r}$	Ω_k, $u\Omega_k$, $v\Omega_k$, $w\Omega_k$, up, vq, Ω_k^2, $(p\Omega_k$, $q\Omega_k$, $pq)$

Terms unique to a configuration in Definition 1 are shown in parentheses.

A response surface experiment design was created using Design-Expert [36] to support estimation of all possible nonlinear and cross model terms up to third-order, which includes each of the terms present in Table 1. A cuboidal I-optimal response surface experiment design [24, 25, 37, 38] was used to specify sets of test points defined by values of $\boldsymbol{v}$, $\boldsymbol{\omega}$, and $\boldsymbol{\Omega}$ at which the multirotor simulation is queried. I-optimal response surface designs minimize the integrated prediction variance across the design space for a given model structure. The data used for modeling were collected in three test blocks, each with 300 test points, to sequentially improve the design by augmenting the previous blocks, meaning that the design points from previous blocks are considered when creating subsequent blocks. A final fourth test block served as validation data withheld from the model identification process; the points were selected from a uniform distribution using a random number generator. A two-dimensional slice of the experiment design is shown in Figure 5, where each block is plotted sequentially (denoted by "$\leq$") to show how the design points progressively fill the design space [39].

The ranges of factor settings used to conduct the experiment are listed in Table 2. The u and v body velocity components as well as the angular velocity bounds were chosen to be operationally representative for the vehicle size. The lower bound on vertical component w was chosen similarly, while the upper bound on w was chosen to be half the hover inflow velocity to avoid regions of flight susceptible to vortex ring state [34]. The bounds on the rotor speeds were chosen from the advance ratio limits of the wind tunnel data for the chosen body velocity limits.

Table 2 Test factor ranges for the multirotor simulation experiment

Factor(s)	Units	Minimum	Maximum
u, v	ft/s	-60	$+60$
w	ft/s	-60	$+8.7$
p, q, r	deg/s	-360	$+360$
$\Omega_1, \Omega_2, \Omega_3, \Omega_4$	rad/s	193	711

V. Modeling Results

Using the queried simulation data from Blocks 1, 2, and 3 of the response surface experiment design, least squares parameter estimates were found for Model 3. A two step approach was used in which least squares regression was first performed independently for each force and moment component to characterize the "best case residuals" as well as the relative importance of terms in the model. Next, a multivariate multiple regression (MMR) approach was used to obtain weighted least-squares parameter estimates for the complete model. The identified model was validated against force and moment data from Block 4 of the response surface experiment design. Furthermore, the relative contributions of each term (regressor times parameter) in the final identified model were evaluated for increasing speeds of steady, forward flight.

A. Regressor Ordering and Initial Regression

First, the equation-error, ordinary least-squares approach was used to estimate the model parameters for each force and moment equation independently (see [4, Ch. 5] and [40, Ch. 6]). The vector

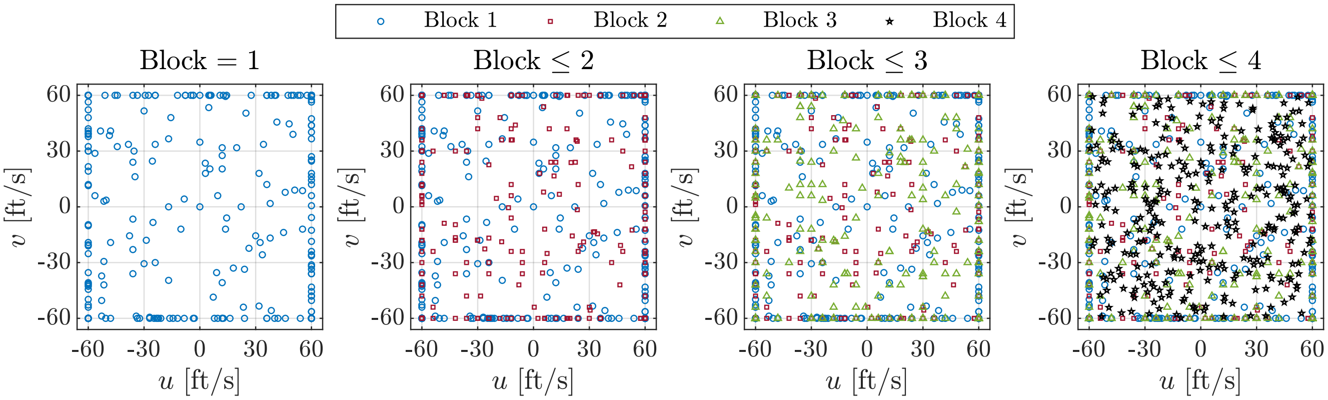

Fig. 5 Two-dimensional slice of the multirotor simulation experiment design.

of N outputs for the ith force/moment equation is

$$\boldsymbol{y}_i = \boldsymbol{X}_i \boldsymbol{\theta}_i, \quad i = 1, \ldots, 6 \tag{38}$$

where $\boldsymbol{\theta}_i \in \mathbb{R}^{p_i}$ is the vector of unknown parameters that appear in the ith equation and $\boldsymbol{X}_i \in \mathbb{R}^{N \times p_i}$ is the matrix of model regressors. Let $\boldsymbol{z}_i$ be the vector of "measured" outputs from the simulation data for the ith force/moment component. Although the outputs at the test points are obtained without error, the underlying wind tunnel data contains random errors which are transferred into $\boldsymbol{z}_i$ in a nonlinear manner. We also recognize there is deterministic residual error between $\boldsymbol{y}_i$ and $\boldsymbol{z}_i$ due to unmodeled aerodynamics. For these reasons, the least-squares solution is not necessarily a minimum mean squared error or maximum likelihood estimate in a statistical sense.

Because the justification for statistical interpretation of the regression results is weak (i.e., the assumptions of a partial F-test do not hold), the coefficient of determination,

$$\mathrm{R}^2 = \frac{\hat{\boldsymbol{y}}^\mathsf{T} \boldsymbol{z} - N\bar{z}^2}{\boldsymbol{z}^\mathsf{T} \boldsymbol{z} - N\bar{z}^2} = 1 - \frac{\mathrm{SS_R}}{\mathrm{SS_T}} \tag{39}$$

was used as the metric in a stepwise regression-like procedure to incrementally add all terms to the model in order of their contribution. Here, $\mathrm{SS_R}$ is the sum of squared residuals and $\mathrm{SS_T}$ is the total sum of squares. A stopping criterion is not considered as typically done in stepwise regression. The aim here is to order terms by their relative importance rather than determine a model structure. That is, all hypothesized terms are eventually included in the model. (A stopping criterion should be used, however, when identifying a model from flight data.) Specifically, consider a linearly parameterized model with p regressors and let $\mathcal{C} = \{\boldsymbol{x}_1, \ldots, \boldsymbol{x}_p\}$, where $\boldsymbol{x}_j$ represents the jth column of the regressor matrix, $\boldsymbol{X}$. The *forward selection ordering algorithm* (FSOA), formally stated in Algorithm 1, begins by considering a model with only one regressor, where denote $\mathcal{I}$ (initially the empty set, $\varnothing$) as the ordered set of regressors already added to the model. Linear regression is performed for the set of regressors $\mathcal{I} \cup \{\boldsymbol{x}_i\}$ for each $\boldsymbol{x}_i \in \mathcal{C}$. The coefficients of determination are computed for each of these identified models and denoted $\mathrm{R}^2(\mathcal{I} \cup \{\boldsymbol{x}_i\})$. The candidate regressor that yields the highest R^2 value is then added to the end of $\mathcal{I}$ and removed from $\mathcal{C}$. This process is repeated until all p terms are included in the ordered set $\mathcal{I}$.

Algorithm 1: FSOA

Input: $\mathcal{C} = \{\boldsymbol{x}_1, \ldots, \boldsymbol{x}_p\}$
Output: $\mathcal{I}$
$\mathcal{I} \leftarrow \varnothing$
while $\mathcal{C} \neq \varnothing$ **do**
  $\boldsymbol{\xi} \leftarrow \arg\max_{\boldsymbol{x} \in \mathcal{C}} \mathrm{R}^2(\mathcal{I} \cup \{\boldsymbol{x}\})$
  $\mathcal{I} \leftarrow \mathcal{I} \cup \{\boldsymbol{\xi}\}$
  $\mathcal{C} \leftarrow \mathcal{C} \setminus \{\boldsymbol{\xi}\}$
end

The FSOA results are given in Tables 3–6, where the boldface values indicate the term that yields the largest R^2 value. Note the R^2 values in Tables 3–6 may be negative, indicating the addition of that term produces a fit worse than a constant model. For each of the models containing all regressors (the last rows of Tables 3-6), the coefficients of determination (R^2), normalized

Table 3 Model 3 X_r and Y_r regressors ordered by relative importance

	R^2 [%]		
Iter.	$C_{H_{\mu_x}}$	$C_{H_{\mu_0,\mu_x}}$	$C_{H_{\mu_x,\mu_z}}$
1	**97.4**	96.6	48.0
2	–	**98.7**	98.3
3	–	–	**99.2**

Table 4 Model 3 Z_r regressors ordered by relative importance

	R^2 [%]			
Iter.	C_{T_0}	$C_{T_{\mu_0}}$	$C_{T_{\mu_x^2}}$	$C_{T_{\mu_z}}$
1	**39.4**	31.3	−14.4	−177.3
2	–	39.7	40.1	**96.5**
3	–	96.7	**98.4**	–
4	–	**98.6**	–	–

Table 5 Model 3 $\mathcal{L}_\mathrm{r}$ and $\mathcal{M}_\mathrm{r}$ regressors ordered by relative importance

	R^2 [%]						
Iter.	$C_{R_{\mu_x}}$	C_{T_0}	$C_{T_{\mu_0}}$	$C_{T_{\mu_z}}$	$C_{H_{\mu_x}}$	$C_{H_{\mu_0,\mu_x}}$	$C_{H_{\mu_x,\mu_z}}$
1	0.5	**83.6**	81.7	13.4	6.5	5.7	0.8
2	84.1	–	83.6	**90.4**	89.8	89.2	84.5
3	90.9	–	90.5	–	**96.4**	95.8	91.3
4	96.8	–	96.4	–	–	96.4	**96.9**
5	**97.3**	–	96.9	–	–	96.9	–
6	–	–	**97.4**	–	–	97.3	–
7	–	–	–	–	–	**97.4**	–

Table 6 Model 3 $\mathcal{N}_\mathrm{r}$ regressors ordered by relative importance

	R^2 [%]					
Iter.	C_{Q_0}	$C_{Q_{\mu_0}}$	$C_{Q_{\mu_z}}$	$C_{Q_{\mu_z^2}}$	$C_{H_{\mu_x}}$	$C_{H_{\mu_x,\mu_z}}$
1	**47.2**	45.8	19.8	0.0	27.8	0.2
2	–	47.2	47.2	47.2	**74.4**	47.5
3	–	74.5	74.4	74.5	–	**74.6**
4	–	**74.7**	74.7	74.7	–	–
5	–	–	74.7	**74.7**	–	–
6	–	–	**74.7**	–	–	–

root mean squared errors (NRMSE),

$$\mathrm{NRMSE} = \frac{1}{\mathrm{range}(\boldsymbol{z})}\sqrt{\frac{1}{N}(\boldsymbol{z}-\hat{\boldsymbol{y}})^\mathsf{T}(\boldsymbol{z}-\hat{\boldsymbol{y}})} \tag{40}$$

and estimated model residual variances,

$$\hat{\sigma}^2 = \frac{1}{N-p}\sum_{k=1}^{N}(z(k)-\hat{y}(k))^2 \tag{41}$$

were computed. These three metrics are given in Table 7 for Model 3.

Table 7 Model 3 initial regression results

Component	R^2 [%]	$\hat{\sigma}^2$	NRMSE [%]
X_r	99.2	1.28×10^{-2}	2.50
Y_r	99.2	1.30×10^{-2}	2.43
Z_r	98.6	5.31×10^{-1}	2.29
$\mathcal{L}_\mathrm{r}$	97.4	1.97×10^{-1}	2.34
$\mathcal{M}_\mathrm{r}$	97.4	1.90×10^{-1}	2.15
$\mathcal{N}_\mathrm{r}$	74.7	2.79×10^{-2}	9.62

Using these results, we can relate each parameter in Model 3 to its definition in Eq. (13) to obtain insight into the predominant physical effects captured by the model. In the X_r and Y_r force components, the most influential model terms are $C_{H_{\mu_x}}\{u,v\}\delta t$, which come from the rotor blade drag coefficient. For example,

$$C_{H_{\mu_x}} u\delta t = \frac{1}{2a}C_\sigma \bar{c}_d u \frac{1}{N_\mathrm{r}}\sum_{i=1}^{N_\mathrm{r}}\Omega_i \tag{42}$$

where $C_{H_{\mu_x}} = \frac{1}{2a}C_\sigma \bar{c}_d$ from Eq. (13) and $\delta t = \frac{1}{N_\mathrm{r}}\sum_{i=1}^{N_\mathrm{r}}\Omega_i$ from Eq. (30). The remaining terms stem from the inflow velocity effects. In the Z_r force equation, the dominant term is $C_{T_0}\delta^2 t$, which comes from the sum of blade-element lift due to rotor speed. This is often the only effect included in control applications. However, we see the subsequent addition of the term containing $C_{T_{\mu_z}}$ significantly increases the R^2 value, indicating its overall importance. In the rolling and pitching moment equations, the most important terms are $C_{T_0}\delta^2\{a,e\}$, which come from the difference in lift due to the difference in rotor speeds (similar to $C_{T_0}\delta^2 t$ in Z_r). Finally, the most significant term in the yawing moment is $C_{Q_0}\delta^2 r$, which models the rotor profile drag due to the difference in rotor speeds [26, Sec. 5-3]. The second most influential term is $C_{H_{\mu_x}}(u\delta a + v\delta e)$, which models the yawing moment due to differential rotor blade drag under virtual aileron and elevator commands (previously mentioned in Section III.B). In the yawing moment, the addition of the final three terms does not appreciably increase the R^2 value. Although blade element theory indicates the presence of these terms, their importance is low for the given simulation data. Overall, these results and this approach, in general, help to inform the model selection process for a given application. It is important to note that the magnitude of the yawing moment data was an order of magnitude smaller than the other moments, thus leading to a lower signal-to-noise ratio, where the "signal" is the part of the yawing moment attributable to regressors and the "noise" is interpreted in the sense described at the beginning of Section V.A.

B. Multivariate Multiple Regression and Validation

Recognizing that parameters are shared among axes, the estimates in Section V.A are not obtained using all data. For example, the parameter $C_{H_{\mu_x}}$ appears in all but the F_z equation, but is estimated five separate times. One approach for reconciling the five distinct estimates of this single parameter is to compute an average of these estimates weighted by the inverse of their variance [41, Ch. 4]:

$$\hat{\theta}_i = \frac{\sum_{j=1}^{p_i}\beta_{ij}\hat{\theta}_{ij}}{\sum_{j=1}^{p_i}\beta_{ij}} \tag{43}$$

where $\beta_{ij} = 1/\sigma_{ij}^2$. The variance of the weighted parameter estimate is then $\sigma_i^2 = 1/\sum_{j=1}^{p_i}\beta_{ij}$. However, Eq. (43) assumes correct parameter variances — a notion that is inconsistent with the deterministic interpretation of the least squares solution. Another approach is to include data from all force and moment components to simultaneously estimate these parameters, which has three main benefits. First, the independent models for each axis may be overfit — especially the rotor aerodynamic moments. This alternative approach reduces the total number of parameters to be identified. Second, all data are used to estimate the set of parameters. For example, $C_{H_{\mu_x}}$ can be estimated using five times as many measurements. Third, as will be detailed shortly, the residuals of the initial deterministic regression in Section V.A can justify a statistical interpretation of the final parameter estimates.

Considering all force and moment components, the output of the kth test point, $\boldsymbol{y}(k) = [y_1(k) \ \cdots \ y_6(k)]^\mathsf{T} \in \mathbb{R}^6$, is

$$\boldsymbol{y}(k) = \boldsymbol{H}(\boldsymbol{v}(k), \boldsymbol{\omega}(k), \boldsymbol{\Omega}(k))\boldsymbol{\theta} \tag{44}$$

where $\boldsymbol{\theta} \in \mathbb{R}^{n_\theta}$ is the vector of proposed parameters and $\boldsymbol{H} : \mathbb{R}^3 \times \mathbb{R}^3 \times \mathbb{R}^{N_\mathrm{r}} \to \mathbb{R}^{6 \times n_\theta}$ is the regressor function for the model. The "measured" output of this model is

$$\boldsymbol{z}(k) = \boldsymbol{y}(k) + \boldsymbol{w}(k) \tag{45}$$

where each $\boldsymbol{w}(k)$ is assumed to be independently sampled from a Gaussian distribution. Let $\tilde{\boldsymbol{w}}(k) = \hat{\boldsymbol{y}}(k) - \boldsymbol{z}(k)$ where $\hat{\boldsymbol{y}}(k) = [\hat{y}_1(k) \ \cdots \ \hat{y}_6(k)]^\mathsf{T}$ was computed through the initial regression in Section V.A. The mean and covariance of $\boldsymbol{w}(k)$ are then respectively approximated by

$$\bar{\boldsymbol{w}} = \mathrm{E}\left\{\boldsymbol{w}(k)\right\} \approx \frac{1}{N}\sum_{j=1}^{N} \tilde{\boldsymbol{w}}(j) \approx \boldsymbol{0} \tag{46a}$$

$$\begin{aligned} \boldsymbol{R} &= \mathrm{E}\left\{[\boldsymbol{w}(k) - \bar{\boldsymbol{w}}][\boldsymbol{w}(k) - \bar{\boldsymbol{w}}]^\mathsf{T}\right\} \\ &\approx \frac{1}{N-1}\sum_{j=1}^{N} \tilde{\boldsymbol{w}}(j)\tilde{\boldsymbol{w}}^\mathsf{T}(j) \end{aligned} \tag{46b}$$

The diagonal elements of $\boldsymbol{R}$ appear in Table 7 as $\hat{\sigma}^2$. The validity of the Gaussian assumption is qualitatively evaluated in Figures 6 and 7 by fitting a Gaussian probability density function to the histogram of residual data and plotting the inverse cumulative distribution function (ICDF), $\Phi^{-1}(P(k))$, against the ordered model residuals. The model residuals appear to follow the shape of a normal distribution (shown as the red line in Figure 6), and the ordered residuals are mostly linear with respect to the ICDF. The "least Gaussian" residuals appear in the Z_r data, where large positive residuals occur with higher probability than a Gaussian distribution would predict. However, Figure 7 shows a straight line is formed by residuals closer to zero, which are more influential in the validity of statistical conclusions [4, Ch. 5]. Altogether, these results indicate normality of the residuals is a reasonable assumption.

With the measurement model determined and random measurement errors characterized, statistical estimates of the model parameters were obtained using MMR [40, Ch. 6]. Let

$$\boldsymbol{\mathcal{Z}} = \begin{bmatrix} \boldsymbol{z}(1) \\ \boldsymbol{z}(2) \\ \vdots \\ \boldsymbol{z}(N) \end{bmatrix}, \boldsymbol{\mathcal{H}} = \begin{bmatrix} \boldsymbol{H}(\boldsymbol{v}(1), \boldsymbol{\omega}(1), \boldsymbol{\Omega}(1)) \\ \boldsymbol{H}(\boldsymbol{v}(2), \boldsymbol{\omega}(2), \boldsymbol{\Omega}(2)) \\ \vdots \\ \boldsymbol{H}(\boldsymbol{v}(N), \boldsymbol{\omega}(N), \boldsymbol{\Omega}(N)) \end{bmatrix}, \boldsymbol{\mathcal{W}} = \begin{bmatrix} \boldsymbol{w}(1) \\ \boldsymbol{w}(2) \\ \vdots \\ \boldsymbol{w}(N) \end{bmatrix} \tag{47}$$

The stacked vector of model outputs is given by $\boldsymbol{\mathcal{Z}} = \boldsymbol{\mathcal{H}}\boldsymbol{\theta} + \boldsymbol{\mathcal{W}}$, and the covariance matrix for $\boldsymbol{\mathcal{W}}$ is $\boldsymbol{\mathcal{R}} = \boldsymbol{R} \otimes \mathbb{I}_N$, where $\otimes$ is the Kronecker product and $\mathbb{I}_N$ is the $N \times N$ identity matrix. The parameter estimates are given by the weighted least squares solution

$$\hat{\boldsymbol{\theta}} = (\boldsymbol{\mathcal{H}}^\mathsf{T}\boldsymbol{\mathcal{R}}^{-1}\boldsymbol{\mathcal{H}})^{-1}\boldsymbol{\mathcal{H}}^\mathsf{T}\boldsymbol{\mathcal{R}}^{-1}\boldsymbol{\mathcal{Z}} \tag{48}$$

and the output of the kth test point is

$$\hat{\boldsymbol{y}}(k) = \boldsymbol{H}(\boldsymbol{v}(k), \boldsymbol{\omega}(k), \boldsymbol{\Omega}(k))\hat{\boldsymbol{\theta}}$$

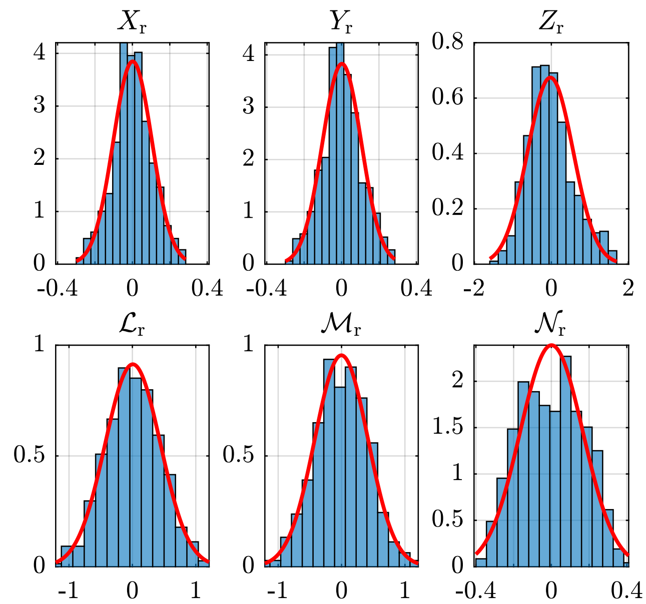

Fig. 6 Probability density of residuals for Model 3.

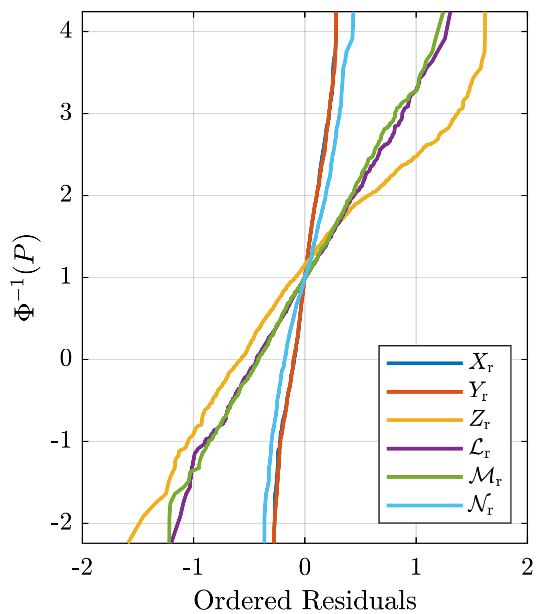

Fig. 7 Normality of residuals for Model 3.

Because each $\boldsymbol{w}(k)$ was assumed to be independently sampled from a Gaussian distribution, these parameter estimates are both minimum mean square error (MMSE) and maximum likelihood (ML) estimates [42, Ch. 2].

The statistical significance of each of the identified parameters is evaluated using the t-statistic,

$$t_{0_j} = \frac{\hat{\theta}_j}{\sigma(\hat{\theta}_j)} \tag{49}$$

where $\sigma(\hat{\theta}_j)$ is the estimated standard deviation of the $\hat{\theta}_j$. The null hypothesis, $H_0 : \hat{\theta}_j = 0$, is rejected with a significance level of α if $|t_{0_j}| > t(\alpha/2, N - n_\theta)$, and the alternate hypothesis, $H_1 : \hat{\theta}_j \neq 0$, is accepted. Here, $t(\alpha/2, N - n_\theta)$ is the sample of a one-tail t-distribution with confidence $\alpha/2$ and $N - n_\theta$ degrees of freedom. Alternatively, the P-value can be used to give the probability of the null hypothesis, H_0 [24, p. 40]:

$$\mathrm{P}\{H_0\} = 2\left(1 - F_t\left(|t_{0_j}|, N - n_\theta\right)\right) \tag{50}$$

where $F_t\left(|t_{0_j}|, N - n_\theta\right)$ is the cumulative distribution function of the $N - n_\theta$ degree-of-freedom one-tail t-distribution evaluated at $|t_{0_j}|$. If $\mathrm{P}\{H_0\} < \alpha$, then H_0 is rejected and θ_j is statistically different from zero.

The MMR results are tabulated in Table 8, where $\mathrm{R}^2_{\mathrm{MMR}}$ and $\mathrm{NRMSE}_{\mathrm{MMR}}$ are the coefficient of determination and normalized root mean square error for the weighted least squares solution, respectively. Another useful measure of model fit included in Table 8 is Theil's inequality coefficient (TIC),

$$\mathrm{TIC}_i = \frac{\sqrt{\frac{1}{N}(\hat{\boldsymbol{y}}_i - \boldsymbol{z}_i)^\mathsf{T}(\hat{\boldsymbol{y}}_i - \boldsymbol{z}_i)}}{\sqrt{\frac{1}{N}\hat{\boldsymbol{y}}_i^\mathsf{T}\hat{\boldsymbol{y}}_i} + \sqrt{\frac{1}{N}\boldsymbol{z}_i^\mathsf{T}\boldsymbol{z}_i}} \tag{51}$$

which is normalized between zero and one with zero indicating perfect fit [40, Ch. 11]. The parameter estimates computed using Eq. (48) are given in Table 9 along with their standard deviation, t-statistic, and P-value. It can be seen that most parameter standard deviations are at least an order of magnitude less than their estimates. The notable exceptions are $C_{Q_{\mu_0}}$, $C_{Q_{\mu_z}}$, and $C_{Q_{\mu_z^2}}$. The lack of statistical significance of these parameters is also evident through their t-statistics and P-values. Although blade element theory indicates the presence of these three terms, their statistical significance is low for the given simulation data. This result indicates these terms are not statistically significant using the available data. However, additional data or sampling approaches may reveal their significance to the yawing moment. Note that the variance-weighted estimates using Eq. (43) resulted in generally similar results to the MMR approach except for $C_{T_{\mu_0}}$ which had a 45% smaller mean but the same standard deviation. It is hypothesized that overfit in the initial regression of the rolling and pitching moments caused this discrepancy.

Table 8 Model 3 MMR results

Component	NRMSE [%]	TIC
X_r	2.55	0.046
Y_r	2.48	0.046
Z_r	2.31	0.035
$\mathcal{L}_\mathrm{r}$	3.77	0.133
$\mathcal{M}_\mathrm{r}$	3.55	0.135
$\mathcal{N}_\mathrm{r}$	9.64	0.272
$\mathrm{R}^2_{\mathrm{MMR}} = 98.4\%$, $\mathrm{NRMSE}_{\mathrm{MMR}} = 1.85\%$		

Finally, the identified models were validated against the force and moment data from Block 4 of the response surface experiment design. The validation metrics are given in Table 10. It can be seen that the axes that validate most poorly as compared to the model fit are the rolling and pitching moments. Due to the moment arm effects of rotor drag forces, these model structures contain the highest number of terms and thus are susceptible to overfit. This observation along with the FSOA results of Section V.A indicate that system identification efforts may benefit from the removal of terms such as $C_{H_{\mu_0,\mu_x}}$ and $C_{T_{\mu_0}}$ from the rolling and pitching moments. These terms did not appreciably increase the coefficient of determination.

Table 9 Model 3 MMR parameter estimates

Parameter	Estimate	Std. Dev.	$\lvert t_0 \rvert$	P-value
$C_{H_{\mu_x}}$	6.38×10^{-3}	1.08×10^{-4}	59.10	0.00
$C_{H_{\mu_0,\mu_x}}$	6.65×10^{-2}	1.68×10^{-3}	39.59	0.00
$C_{H_{\mu_x,\mu_z}}$	-1.05×10^{-2}	3.16×10^{-4}	33.14	0.00
C_{T_0}	1.48×10^{-2}	1.44×10^{-4}	102.65	0.00
$C_{T_{\mu_0}}$	3.29×10^{-2}	3.53×10^{-3}	9.33	0.00
$C_{T_{\mu_x^2}}$	4.57×10^{-2}	1.50×10^{-3}	30.51	0.00
$C_{T_{\mu_z}}$	-7.05×10^{-2}	3.85×10^{-4}	182.94	0.00
$C_{R_{\mu_x}}$	1.14×10^{-2}	8.22×10^{-4}	13.88	0.00
C_{Q_0}	1.31×10^{-3}	2.59×10^{-4}	5.08	3.91×10^{-7}
$C_{Q_{\mu_0}}$	-5.12×10^{-3}	7.70×10^{-3}	0.67	5.06×10^{-1}
$C_{Q_{\mu_z}}$	-3.49×10^{-4}	7.74×10^{-4}	0.45	6.51×10^{-1}
$C_{Q_{\mu_z^2}}$	6.22×10^{-2}	1.06×10^{-1}	0.59	5.57×10^{-1}

Table 10 Model 3 validation metrics

Component	$\hat{\sigma}^2$	NRMSE [%]	TIC
X_r	1.04×10^{-2}	2.26	0.046
Y_r	9.50×10^{-3}	2.00	0.045
Z_r	3.97×10^{-1}	2.84	0.042
$\mathcal{L}_\mathrm{r}$	2.86×10^{-1}	5.14	0.158
$\mathcal{M}_\mathrm{r}$	2.76×10^{-1}	4.68	0.148
$\mathcal{N}_\mathrm{r}$	1.75×10^{-2}	9.52	0.291

C. Steady Flight Analysis

The regressor importance analysis in Section V.A is based on the ensemble of data across a broad range of conditions. For motion in the neighborhood of some nominal flight condition, however, the relative importance of regressors may differ. For this reason, we also consider the relative contributions of model terms (regressors times parameters) through increasing speeds of forward flight.

Using the high-fidelity simulation environment described in [23, 28], the family of equilibrium constant altitude, forward flight conditions was numerically determined for airspeeds ranging from zero to 60 ft/s. Next, the normalized contributions of model terms across these forward flight conditions were evaluated. For the ith force/moment component, let the jth term be denoted $y_{ij} = h_{ij}\theta_j$, where h_{ij} is the i, j-element of the regressor matrix $\boldsymbol{H}$ in Eq. (44). Since these steady motions are characterized by zero applied moment and side-force, we qualitatively evaluate the normalized contributions of modeled terms $\hat{X}_{\mathrm{r},j}$ and $\hat{Z}_{\mathrm{r},j}$ in the X_r and Z_r forces as shown in Figures 8 and 9, respectively.

For the X_r force component, the most important term across all forward flight conditions is $C_{H_{\mu_x}} u\delta t$, which is in agreement with the FSOA results. Additionally, we see that as airspeed increases,

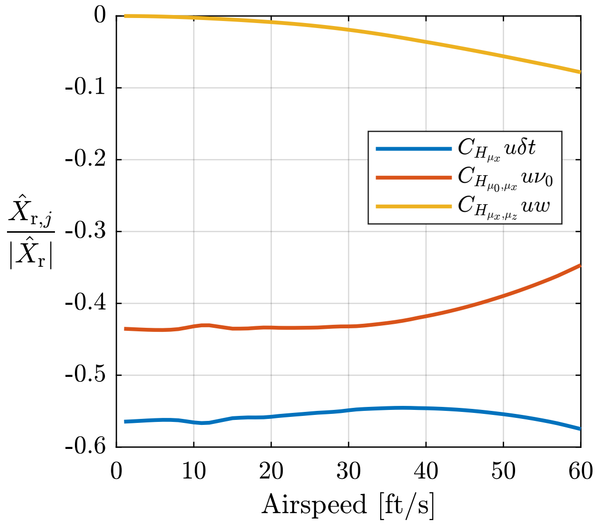

Fig. 8 X_{r} **model term contributions in forward flight.**

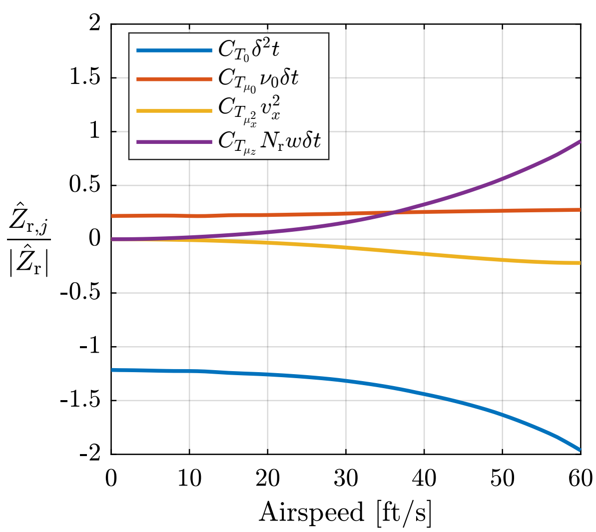

Fig. 9 Z_{r} **model term contributions in forward flight.**

the importance of the term $C_{H_{\mu_x,\mu_z}} uw$ increases, which may be relevant control and estimation applications involving flight at high speeds. The Z_{r} force component tells a more interesting story. Again, the most important term, $C_{T_0}\delta^2 t$, agrees with the FSOA results. However, the magnitude of $C_{T_{\mu_z}}(N_{\mathrm{r}} w\delta t - \Delta\nu_Z)$ (one of the least important terms at low speeds) substantially increases with airspeed. This term captures the reduction in total thrust as airspeed increases, requiring increased rotor speeds to maintain level flight. The intersection of curves in Figure 9 represents forward speeds at which the relative importance of terms changes.

VI. Conclusions

Multirotor flight dynamic models for control and estimation have typically been limited to a small operating domain. In this work, we addressed this issue by carefully incorporating established rotor aerodynamic theory into models that can be identified from flight data. Building on blade-element and momentum theory while carefully presenting the underlying assumptions, we derived a compact but accurate nonlinear flight dynamic model. Additional assumptions led to further simplified models that can more easily be identified from experimental data and used in control and estimation applications. While the proposed models capture important physical effects that are absent in simpler models, some of the assumptions, such as uniform inflow conditions and steady-flight blade element loads, may limit its applicability for more extreme flight regimes or motion on fast time scales.

To ensure reliable parameter identification, design of experiments and response surface methodology were employed, generating a set of test points for a high-fidelity simulation study. The modeling results not only reveal relative significance of model regressors through a forward selection-like algorithm, but also statistically inform a two-step procedure for identifying model parameters using all force and moment data. The model fit and predictive skill of the derived models were validated, demonstrating the utility of the physics-based model structure. Finally, by examining the relative contribution of individual terms over a range of forward-flight speeds, we have shown which effects may or may not be critical for a given application, thereby informing a hierarchical approach to model selection that can be used in conjunction with data-driven model structure determination techniques.

Appendix: Derivation of Model 1

We begin by computing the rigid body force vector (22) using the rotor force components in Eq. (15) evaluated at the local rotor velocities, $\boldsymbol{v}_i$, as approximated by Eq. (27).

$$X_{\mathrm{r}} = \rho\pi R^2 u \sum_{i=1}^{N_{\mathrm{r}}} \Big(-C_{H_{\mu_x}} R\Omega_i - C_{H_{\mu_0,\mu_x}} \nu_0 - C_{H_{\mu_x^2}} v_x - C_{H_{\mu_x,\mu_z}} (w + p y_i - q x_i) \Big) \tag{A.1a}$$

$$Y_{\mathrm{r}} = \rho\pi R^2 v \sum_{i=1}^{N_{\mathrm{r}}} \Big(-C_{H_{\mu_x}} R\Omega_i - C_{H_{\mu_0,\mu_x}} \nu_0 - C_{H_{\mu_x^2}} v_x - C_{H_{\mu_x,\mu_z}} (w + p y_i - q x_i) \Big) \tag{A.1b}$$

$$Z_{\mathrm{r}} = \rho\pi R^2 \sum_{i=1}^{N_{\mathrm{r}}} \Big(-C_{T_0} R^2 \Omega_i^2 + C_{T_{\mu_0}} R\nu_0\Omega_i - C_{T_{\mu_x}} R v_x \Omega_i + C_{T_{\mu_z}} R(w + p y_i - q x_i)\Omega_i - C_{T_{\mu_x^2}} v_x^2 \Big) \tag{A.1c}$$

Recall from the virtual actuator definitions in Eqs. (28) and (30) that $\delta^2 t = \frac{1}{N_{\mathrm{r}}}\sum_{i=1}^{N_{\mathrm{r}}} \Omega_i^2$, $\delta t = \frac{1}{N_{\mathrm{r}}}\sum_{i=1}^{N_{\mathrm{r}}} \Omega_i$, $\delta a = -\sum_{i=1}^{N_{\mathrm{r}}} y_i \Omega_i$, and $\delta e = \sum_{i=1}^{N_{\mathrm{r}}} x_i \Omega_i$. Additionally, Assumption 4c implies $\sum_{i=1}^{N_{\mathrm{r}}} x_i = \sum_{i=1}^{N_{\mathrm{r}}} y_i = 0$. Thus, Eq. (A.1) reduces to

$$X_{\mathrm{r}} = \rho\pi R^2 N_{\mathrm{r}} u \Big(-C_{H_{\mu_x}} R\delta t - C_{H_{\mu_0,\mu_x}} \nu_0 + C_{H_{\mu_x^2}} v_x - C_{H_{\mu_x,\mu_z}} w \Big) \tag{A.2a}$$

$$Y_{\mathrm{r}} = \rho\pi R^2 N_{\mathrm{r}} v \Big(-C_{H_{\mu_x}} R\delta t - C_{H_{\mu_0,\mu_x}} \nu_0 + C_{H_{\mu_x^2}} v_x - C_{H_{\mu_x,\mu_z}} w \Big) \tag{A.2b}$$

$$Z_{\mathrm{r}} = \rho\pi R^2 \Big(-C_{T_0} R^2 N_{\mathrm{r}} \delta^2 t + C_{T_{\mu_0}} R N_{\mathrm{r}} \nu_0 \delta t - C_{T_{\mu_x}} R N_{\mathrm{r}} v_x \delta t + C_{T_{\mu_z}} R(N_{\mathrm{r}} w\delta t - \Delta\nu_Z) - C_{T_{\mu_x^2}} N_{\mathrm{r}} v_x^2 \Big) \tag{A.2c}$$

Finally, adding the airframe force $\boldsymbol{F}_{\mathrm{a}}$, we obtain the force components in Model 1.

Recall from Eq. (23), the total rotor-based moment about the body frame origin is the sum of the rotor moments plus the sum of the moments due to the rotor forces. We first write the components of the moment vector due to rotor aerodynamic moments, given by Eq. (19), as

$$-\sum_{i=1}^{N_{\mathrm{r}}}\sigma_i\mathcal{L}_{\mathrm{r},i} = \rho\pi R^2\sum_{i=1}^{N_{\mathrm{r}}}\sigma_i\Big(C_{R_{\mu_x}}R^2\Omega_i u - C_{R_{\mu_0,\mu_x}}R\nu_0 u + C_{R_{\mu_x^2}}Rv_x u - C_{R_{\mu_x,\mu_z}}Ru(w+py_i-qx_i)\Big) \tag{A.3a}$$

$$-\sum_{i=1}^{N_{\mathrm{r}}}\sigma_i\mathcal{M}_{\mathrm{r},i} = \rho\pi R^2\sum_{i=1}^{N_{\mathrm{r}}}\sigma_i\Big(C_{R_{\mu_x}}R^2\Omega_i v - C_{R_{\mu_0,\mu_x}}R\nu_0 v + C_{R_{\mu_x^2}}Rv_x v - C_{R_{\mu_x,\mu_z}}Rv(w+py_i-qx_i)\Big) \tag{A.3b}$$

$$\begin{aligned}-\sum_{i=1}^{N_{\mathrm{r}}}\sigma_i\mathcal{N}_{\mathrm{r},i} = \rho\pi R^2\sum_{i=1}^{N_{\mathrm{r}}}\sigma_i\Big(&-C_{Q_0}R^3\Omega_i^2 - C_{Q_{\mu_0}}R^2\nu_0\Omega_i + C_{Q_{\mu_x}}R^2v_x\Omega_i - C_{Q_{\mu_z}}R^2(w+py_i-qx_i)\Omega_i\\ &+ C_{Q_{\mu_0^2}}R\nu_0^2 + C_{Q_{\mu_x^2}}Rv_x^2 + C_{Q_{\mu_z^2}}R(w+py_i-qx_i)^2\\ &- C_{Q_{\mu_0,\mu_x}}R\nu_0 v_x + C_{Q_{\mu_0,\mu_z}}R\nu_0(w+py_i-qx_i) - C_{Q_{\mu_x,\mu_z}}Rv_x(w+py_i-qx_i)\Big)\end{aligned} \tag{A.3c}$$

By Assumption 4b, $\sum_{i=1}^{N_{\mathrm{r}}}\sigma_i = 0$. Additionally, the combination of Assumptions 4a, 4c, and 4d imply $\sum_{i=1}^{N_{\mathrm{r}}}\sigma_i x_i = \sum_{i=1}^{N_{\mathrm{r}}}\sigma_i y_i = 0$. Therefore, we have

$$-\sum_{i=1}^{N_{\mathrm{r}}}\sigma_i\mathcal{L}_{\mathrm{r},i} = \rho\pi R^2\Big(C_{R_{\mu_x}}R^2u\textstyle\sum_{i=1}^{N_{\mathrm{r}}}\sigma_i\Omega_i\Big) \tag{A.4a}$$

$$-\sum_{i=1}^{N_{\mathrm{r}}}\sigma_i\mathcal{M}_{\mathrm{r},i} = \rho\pi R^2\Big(C_{R_{\mu_x}}R^2v\textstyle\sum_{i=1}^{N_{\mathrm{r}}}\sigma_i\Omega_i\Big) \tag{A.4b}$$

$$-\sum_{i=1}^{N_{\mathrm{r}}}\sigma_i\mathcal{N}_{\mathrm{r},i} = \rho\pi R^2\sum_{i=1}^{N_{\mathrm{r}}}\sigma_i\Big(-C_{Q_0}R^3\Omega_i^2 - C_{Q_{\mu_0}}R^2\nu_0\Omega_i + C_{Q_{\mu_x}}R^2v_x\Omega_i - C_{Q_{\mu_z}}R^2(w+py_i-qx_i)\Omega_i + C_{Q_{\mu_z^2}}R(py_i-qx_i)^2\Big) \tag{A.4c}$$

From the virtual actuator definitions in Eqs. (28) and (30), $\delta^2 r = -\sum_{i=1}^{N_{\mathrm{r}}}\sigma_i\Omega_i^2$ and $\delta r = -\sum_{i=1}^{N_{\mathrm{r}}}\sigma_i\Omega_i$. Thus,

$$-\sum_{i=1}^{N_{\mathrm{r}}}\sigma_i\mathcal{L}_{\mathrm{r},i} = \rho\pi R^2\left(-C_{R_{\mu_x}}R^2u\delta r\right) \tag{A.5a}$$

$$-\sum_{i=1}^{N_{\mathrm{r}}}\sigma_i\mathcal{M}_{\mathrm{r},i} = \rho\pi R^2\left(-C_{R_{\mu_x}}R^2v\delta r\right) \tag{A.5b}$$

$$-\sum_{i=1}^{N_{\mathrm{r}}}\sigma_i\mathcal{N}_{\mathrm{r},i} = \rho\pi R^2\Big(C_{Q_0}R^3\delta^2 r + C_{Q_{\mu_0}}R^2\nu_0\delta r - C_{Q_{\mu_x}}R^2v_x\delta r + C_{Q_{\mu_z}}R^2\big(w\delta r - \Delta\nu_w\big) - C_{Q_{\mu_z^2}}R\Delta\nu_{\mathcal{N}}^2\Big) \tag{A.5c}$$

where

$$\Delta\nu_{\mathcal{N}} \coloneqq \textstyle\sum_{i=1}^{N_{\mathrm{r}}}\sigma_i(py_i-qx_i)\Omega_i \tag{A.6}$$

$$\Delta\nu_{\mathcal{N}}^2 \coloneqq -\textstyle\sum_{i=1}^{N_{\mathrm{r}}}\sigma_i(py_i-qx_i)^2 \tag{A.7}$$

Next, we compute the contribution of rotor forces to the total aerodynamic moment

$$\sum_{i=1}^{N_{\mathrm{r}}}\boldsymbol{p}_i\times\boldsymbol{F}_{\mathrm{r},i} = \sum_{i=1}^{N_{\mathrm{r}}}\begin{bmatrix} y_iZ_{\mathrm{r},i}+hY_{\mathrm{r},i}\\ -x_iZ_{\mathrm{r},i}-hX_{\mathrm{r},i}\\ x_iY_{\mathrm{r},i}-y_iX_{\mathrm{r},i}\end{bmatrix}$$

where we have made use of Assumption 4e that $z_i = -h$. Using the rotor force components from Eq. 15 evaluated at the local rotor velocities, it follows that

$$\begin{aligned}\sum_{i=1}^{N_{\mathrm{r}}}(y_iZ_{\mathrm{r},i}+hY_{\mathrm{r},i}) = \rho\pi R^2\sum_{i=1}^{N_{\mathrm{r}}}\Big(&-C_{T_0}R^2y_i\Omega_i^2 + C_{T_{\mu_0}}R\nu_0 y_i\Omega_i - C_{T_{\mu_x}}Rv_xy_i\Omega_i + C_{T_{\mu_z}}Ry_i(w+py_i-qx_i)\Omega_i\\ &- C_{T_{\mu_x^2}}v_x^2y_i - C_{H_{\mu_x}}Rh\Omega_i v - C_{H_{\mu_0,\mu_x}}h\nu_0 v + C_{H_{\mu_x^2}}hv_xv - C_{H_{\mu_x,\mu_z}}hv(w+py_i-qx_i)\Big)\end{aligned} \tag{A.8a}$$

$$\begin{aligned}\sum_{i=1}^{N_{\mathrm{r}}}(-x_iZ_{\mathrm{r},i}-hX_{\mathrm{r},i}) = \rho\pi R^2\sum_{i=1}^{N_{\mathrm{r}}}\Big(&C_{T_0}R^2x_i\Omega_i^2 - C_{T_{\mu_0}}R\nu_0x_i\Omega_i + C_{T_{\mu_x}}Rv_xx_i\Omega_i - C_{T_{\mu_z}}Rx_i(w+py_i-qx_i)\Omega_i\\ &+ C_{T_{\mu_x^2}}v_x^2x_i + C_{H_{\mu_x}}Rh\Omega_i u + C_{H_{\mu_0,\mu_x}}h\nu_0u - C_{H_{\mu_x^2}}hv_xu + C_{H_{\mu_x,\mu_z}}hu(w+py_i-qx_i)\Big)\end{aligned} \tag{A.8b}$$

$$\begin{aligned}\sum_{i=1}^{N_{\mathrm{r}}}(x_iY_{\mathrm{r},i}-y_iX_{\mathrm{r},i}) = \rho\pi R^2\sum_{i=1}^{N_{\mathrm{r}}}\Big(&C_{H_{\mu_x}}R(uy_i-vx_i)\Omega_i + C_{H_{\mu_0,\mu_x}}\nu_0(uy_i-vx_i) + C_{H_{\mu_x,\mu_z}}(uy_i-vx_i)(w+py_i-qx_i)\\ &+ C_{H_{\mu_x^2}}v_x(uy_i-vx_i)\Big)\end{aligned} \tag{A.8c}$$

Recall, Assumption 4c implies $\sum_{i=1}^{N_{\mathrm{r}}}x_i = \sum_{i=1}^{N_{\mathrm{r}}}y_i = 0$. Furthermore, Assumptions 4c and 4d together imply $\sum_{i=1}^{N_{\mathrm{r}}}x_iy_i = 0$ and $\sum_{i=1}^{N_{\mathrm{r}}}x_i^2 = \sum_{i=1}^{N_{\mathrm{r}}}y_i^2 = \frac{1}{2}N_{\mathrm{r}}\ell^2$. Using these facts and the virtual actuator definitions, Eq. (A.8) simplifies to

$$\begin{aligned}\sum_{i=1}^{N_{\mathrm{r}}}(y_iZ_{\mathrm{r},i}+hY_{\mathrm{r},i}) = \rho\pi R^2\Big(&C_{T_0}R^2\delta^2a - C_{T_{\mu_0}}R\nu_0\delta a + C_{T_{\mu_x}}Rv_x\delta a - C_{T_{\mu_z}}R\big(w\delta a - \Delta\nu_{\mathcal{L}}\big)\\ &- C_{H_{\mu_x}}RN_{\mathrm{r}}hv\delta t - C_{H_{\mu_0,\mu_x}}N_{\mathrm{r}}h\nu_0v - C_{H_{\mu_x,\mu_z}}N_{\mathrm{r}}hvw - C_{H_{\mu_x^2}}N_{\mathrm{r}}hv_xv\Big)\end{aligned} \tag{A.9a}$$

$$\begin{aligned}\sum_{i=1}^{N_{\mathrm{r}}}(-x_iZ_{\mathrm{r},i}-hX_{\mathrm{r},i}) = \rho\pi R^2\Big(&C_{T_0}R^2\delta^2e - C_{T_{\mu_0}}R\nu_0\delta e + C_{T_{\mu_x}}Rv_x\delta e - C_{T_{\mu_z}}R\big(w\delta e - \Delta\nu_{\mathcal{M}}\big)\\ &+ C_{H_{\mu_x}}RN_{\mathrm{r}}hu\delta t + C_{H_{\mu_0,\mu_x}}N_{\mathrm{r}}h\nu_0u + C_{H_{\mu_x,\mu_z}}N_{\mathrm{r}}huw + C_{H_{\mu_x^2}}N_{\mathrm{r}}hv_xu\Big)\end{aligned} \tag{A.9b}$$

$$\sum_{i=1}^{N_\mathrm{r}}(x_i Y_{\mathrm{r},i} - y_i X_{\mathrm{r},i}) = \rho\pi R^2\Big(-C_{H_{\mu_x}} R(u\delta a + v\delta e) + \tfrac{1}{2} C_{H_{\mu_x,\mu_z}} N_\mathrm{r}\ell^2(up+vq)\Big) \quad \text{(A.9c)}$$

where
$$\Delta\nu_\mathcal{L} \coloneqq \textstyle\sum_{i=1}^{N_\mathrm{r}} y_i(py_i - qx_i)\Omega_i \quad \text{(A.10)}$$
$$\Delta\nu_\mathcal{M} \coloneqq \textstyle\sum_{i=1}^{N_\mathrm{r}} x_i(qx_i - py_i)\Omega_i \quad \text{(A.11)}$$

Altogether, Eqs. (A.5) and (A.9) are substituted into the total rotor-based aerodynamic moment given by Eq. (23) to obtain

$$\begin{aligned}\mathcal{L}_\mathrm{r} = \rho\pi R^2\Big(&-C_{R_{\mu_x}} R^2 u\delta r + C_{T_0} R^2\delta^2 a - C_{T_{\mu_0}} R\nu_0\delta a \\ &+ C_{T_{\mu_x}} Rv_x\delta a - C_{T_{\mu_z}} R\big(w\delta a - \Delta\nu_\mathcal{L}\big) \\ &- C_{H_{\mu_x}} RN_\mathrm{r}hv\delta t - C_{H_{\mu_0,\mu_x}} N_\mathrm{r}hv\nu_0 \\ &+ C_{H_{\mu_x^2}} N_\mathrm{r}hvv_x - C_{H_{\mu_x,\mu_z}} N_\mathrm{r}hvw\Big) \quad \text{(A.12a)}\end{aligned}$$

$$\begin{aligned}\mathcal{M}_\mathrm{r} = \rho\pi R^2\Big(&-C_{R_{\mu_x}} R^2 v\delta r + C_{T_0} R^2\delta^2 e - C_{T_{\mu_0}} R\nu_0\delta e \\ &+ C_{T_{\mu_x}} Rv_x\delta e - C_{T_{\mu_z}} R\big(w\delta e - \Delta\nu_\mathcal{M}\big) \\ &+ C_{H_{\mu_x}} RN_\mathrm{r}hu\delta t + C_{H_{\mu_0,\mu_x}} N_\mathrm{r}hu\nu_0 \\ &- C_{H_{\mu_x^2}} N_\mathrm{r}huv_x + C_{H_{\mu_x,\mu_z}} N_\mathrm{r}huw\Big) \quad \text{(A.12b)}\end{aligned}$$

$$\begin{aligned}\mathcal{N}_\mathrm{r} = \rho\pi R^2\Big(&C_{Q_0} R^3\delta^2 r + C_{Q_{\mu_0}} R^2\nu_0\delta r - C_{Q_{\mu_x}} R^2 v_x\delta r \\ &+ C_{Q_{\mu_z}} R^2\Big(w\delta r - \Delta\nu_\mathcal{N}\Big) - C_{Q_{\mu_z^2}} R\Delta\nu_\mathcal{N}^2 \\ &- C_{H_{\mu_x}} R(u\delta a + v\delta e) + \tfrac{1}{2} C_{H_{\mu_x,\mu_z}} N_\mathrm{r}\ell^2(up+vq)\Big) \quad \text{(A.12c)}\end{aligned}$$

The airframe and gyroscopic moments are added to Eq. (A.12) according to Eq. (25) to yield the moment components given in Model 1.

Finally, we derive expressions for $\Delta\nu_\mathcal{L}$, $\Delta\nu_\mathcal{M}$, $\Delta\nu_\mathcal{N}$, and $\Delta\nu_\mathcal{N}^2$ in terms of virtual actuators and show how their expressions depend on the class of configurations given in Definition 1. It turns out the structure of $\mathbf{M_{ix}}$ under Assumption 4 allows us to readily compute its pseudoinverse. First, notice that Assumption 4 implies $\mathbf{M_{ix}}$ can be written as

$$\mathbf{M_{ix}} = \begin{bmatrix} \frac{1}{N_\mathrm{r}} & \frac{1}{N_\mathrm{r}} & \cdots & \frac{1}{N_\mathrm{r}} & \frac{1}{N_\mathrm{r}} \\ -\ell\sin\theta_1 & -\ell\sin\theta_2 & \cdots & -\ell\sin\theta_{N_\mathrm{r}-1} & -\ell\sin\theta_{N_\mathrm{r}} \\ \ell\cos\theta_1 & \ell\cos\theta_2 & \cdots & \ell\cos\theta_{N_\mathrm{r}-1} & \ell\cos\theta_{N_\mathrm{r}} \\ -1 & +1 & \cdots & -1 & +1 \end{bmatrix} \quad \text{(A.13)}$$

where θ_i is the angle from the $\boldsymbol{b}_1$ axis of the ith rotor arm. Therefore, $\mathbf{M_{ix}}\mathbf{M_{ix}^\mathsf{T}}$ is written as shown in Eq. (A.14), where the sum, $\sum$, is from $i = 1$ to N_r. By the symmetry implied by Assumption 4,

$$\mathbf{M_{ix}}\mathbf{M_{ix}^\mathsf{T}} = \mathbf{diag}\left(\frac{1}{N_\mathrm{r}}, \frac{N_\mathrm{r}}{2}\ell^2, \frac{N_\mathrm{r}}{2}\ell^2, N_\mathrm{r}\right)$$
$$\implies \left(\mathbf{M_{ix}}\mathbf{M_{ix}^\mathsf{T}}\right)^{-1} = \mathbf{diag}\left(N_\mathrm{r}, \frac{2}{N_\mathrm{r}\ell^2}, \frac{2}{N_\mathrm{r}\ell^2}, \frac{1}{N_\mathrm{r}}\right) \quad \text{(A.15)}$$

Finally, the pseudoinverse of $\mathbf{M_{ix}}$ is

$$\mathbf{M_{ix}^\dagger} = \mathbf{M_{ix}^\mathsf{T}}\mathbf{diag}\left(N_\mathrm{r}, \frac{2}{N_\mathrm{r}\ell^2}, \frac{2}{N_\mathrm{r}\ell^2}, \frac{1}{N_\mathrm{r}}\right) \quad \text{(A.16)}$$

Consider the configuration-dependent term $\Delta\nu_\mathcal{L} \coloneqq \sum_{i=1}^{N_\mathrm{r}} y_i(py_i - qx_i)\Omega_i$. Using Eq. (A.16), we have

$$\begin{aligned}\Delta\nu_\mathcal{L} &\coloneqq \sum_{i=1}^{N_\mathrm{r}} y_i(py_i - qx_i)\Omega_i \quad \text{(A.17a)} \\ &= \sum_{i=1}^{N_\mathrm{r}} \ell\sin\theta_i(p\ell\sin\theta_i - q\ell\cos\theta_i)(\delta t - \delta a\frac{2}{N_\mathrm{r}\ell}\sin\theta_i \\ &\qquad + \delta e\frac{2}{N_\mathrm{r}\ell}\cos\theta_i - \frac{1}{N_\mathrm{r}}\delta r(-1)^{i-1}) \quad \text{(A.17b)} \\ &= p\ell^2\delta t\sum\sin^2\theta_i - p\ell^2\frac{1}{N_\mathrm{r}}\delta r\sum(-1)^{i-1}\sin^2\theta_i \\ &\qquad + q\frac{\ell^2}{2}\frac{1}{N_\mathrm{r}}\delta r\sum(-1)^{i-1}\sin(2\theta_i) \\ &\qquad - q\frac{\ell^2}{2}\delta t\sum\sin(2\theta_i) - p\frac{\ell}{2}(\delta a\sum\sin^3\theta_i \\ &\qquad\qquad - \delta e\sum\sin^2\theta_i\cos\theta_i) \\ &\qquad + q\frac{\ell}{2}(\delta a\sum\sin^2\theta_i\cos\theta_i - \delta e\sum\sin\theta_i\cos^2\theta_i) \quad \text{(A.17c)}\end{aligned}$$

By Assumption 4, the last three terms in Eq. (A.17c) vanish. Thus, we have

$$\begin{aligned}\Delta\nu_\mathcal{L} = \frac{1}{2}\ell^2 pN_\mathrm{r}\delta t - p\ell^2\frac{1}{N_\mathrm{r}}\delta r\sum(-1)^{i-1}\sin^2\theta_i \\ + q\frac{\ell^2}{2}\frac{1}{N_\mathrm{r}}\delta r\sum(-1)^{i-1}\sin(2\theta_i) \quad \text{(A.18)}\end{aligned}$$

The second two terms in Eq. (A.18) are zero for $N_\mathrm{r} \geq 6$. For $N_\mathrm{r} = 4$, they are $\frac{1}{2}\ell^2\left(p\cos(2\theta_0) + q\sin(2\theta_0)\right)\delta r$, where θ_0 is either zero (+ configuration) or π/N_r ($\times$ configuration). Finally using Definition 1,

$$\Delta\nu_\mathcal{L} = \begin{cases} \frac{1}{2}\ell^2 p(N_\mathrm{r}\delta t - \delta r) & \text{quadrotor}_+ \\ \frac{1}{2}\ell^2(N_\mathrm{r}p\delta t + q\delta r) & \text{quadrotor}_\times \\ \frac{1}{2}\ell^2 pN_\mathrm{r}\delta t & \text{multirotor}_{\geq 6} \end{cases} \quad \text{(A.19)}$$

The remainder of the configuration-dependent terms are found similarly. □

Acknowledgments

The first and third authors gratefully acknowledge the support of NASA under Grant No. 80NSSC20M0162 and the Commonwealth Center for Innovation in Autonomous Systems (C2IAS), Virginia Innovation Partnership Corporation (VIPC). The first, third, and fourth authors also gratefully acknowledge the support of the United States Air Force under grant No. FA865123CA019.

$$\mathbf{M_{ix}}\mathbf{M_{ix}^\mathsf{T}} = \begin{bmatrix} \frac{1}{N_\mathrm{r}} & -\frac{\ell}{N_\mathrm{r}}\sum\cos\theta_i & \frac{\ell}{N_\mathrm{r}}\sum\sin\theta_i & 0 \\ -\frac{\ell}{N_\mathrm{r}}\sum\cos\theta_i & \ell^2\sum\cos^2\theta_i & -\frac{\ell}{2}\sum\sin(2\theta_i) & \ell\sum(-1)^{i-1}\cos\theta_i \\ \frac{\ell}{N_\mathrm{r}}\sum\sin\theta_i & -\frac{\ell}{2}\sum\sin(2\theta_i) & \ell^2\sum\sin^2\theta_i & -\ell\sum(-1)^{i-1}\sin\theta_i \\ 0 & \ell\sum(-1)^{i-1}\cos\theta_i & -\ell\sum(-1)^{i-1}\sin\theta_i & N_\mathrm{r} \end{bmatrix} \quad \text{(A.14)}$$

References

[1] Cooper, J., Hopwood, J. W., Woolsey, C. A., De Wekker, S. F. J., and DeVore, M., "Intelligent Wind Estimation for Chemical Source Localization," *79th Annual Forum & Technology Display*, Vertical Flight Society, West Palm Beach, FL, 2023-05-16/2023-05-18, pp. 1–20. https://doi.org/10.4050/F-0079-2023-18194.

[2] Smeur, E. J. J., Chu, Q., and de Croon, G. C. H. E., "Adaptive Incremental Nonlinear Dynamic Inversion for Attitude Control of Micro Air Vehicles," *Journal of Guidance, Control, and Dynamics*, Vol. 39, No. 3, 2016, pp. 450–461. https://doi.org/10.2514/1.G001490.

[3] Grauer, J. A., and Morelli, E. A., "Generic Global Aerodynamic Model for Aircraft," *Journal of Aircraft*, Vol. 52, No. 1, 2015, pp. 13–20. https://doi.org/10.2514/1.C032888.

[4] Morelli, E. A., and Klein, V., *Aircraft System Identification: Theory and Practice*, 2nd ed., Sunflyte Enterprises, Williamsburg, Virginia, 2016.

[5] Simmons, B. M., Gresham, J. L., and Woolsey, C. A., "Aero-Propulsive Modeling for Propeller Aircraft Using Flight Data," *Journal of Aircraft*, Vol. 60, No. 1, 2023, pp. 81–96. https://doi.org/10.2514/1.C036773.

[6] Peters, D. A., and He, C. J., "Finite State Induced Flow Models Part II: Three-dimensional Rotor Disk," *Journal of Aircraft*, Vol. 32, No. 2, 1995, pp. 323–333. https://doi.org/10.2514/3.46719.

[7] Miller, R. H., "Unsteady Air Loads on Helicopter Rotor Blades," *The Journal of the Royal Aeronautical Society*, Vol. 68, No. 640, 1964, pp. 217–229. https://doi.org/10.1017/S0001924000060887.

[8] Barcelos, D., Kolaei, A., and Bramesfeld, G., "Aerodynamic Interactions of Quadrotor Configurations," *Journal of Aircraft*, Vol. 57, No. 6, 2020, pp. 1074–1090. https://doi.org/10.2514/1.C035614.

[9] Niermeyer, P., Raffler, T., and Holzapfel, F., "Open-Loop Quadrotor Flight Dynamics Identification in Frequency Domain via Closed-Loop Flight Testing," *AIAA Guidance, Navigation, and Control Conference*, American Institute of Aeronautics and Astronautics, Kissimmee, Florida, 2015, p. 14. https://doi.org/10.2514/6.2015-1539.

[10] Alabsi, M. I., and Fields, T. D., "Real-Time Closed-Loop System Identification of a Quadcopter," *Journal of Aircraft*, Vol. 56, No. 1, 2019, pp. 324–335. https://doi.org/10.2514/1.C034219.

[11] Cunningham, M. A., and Hubbard, J. E., "Open-Loop Linear Model Identification of a Multirotor Vehicle with Active Feedback Control," *Journal of Aircraft*, Vol. 57, No. 6, 2020, pp. 1044–1061. https://doi.org/10.2514/1.C035834.

[12] Ivler, C. M., Rowe, E. S., Martin, J., Lopez, M. J., and Tischler, M. B., "System Identification Guidance for Multirotor Aircraft: Dynamic Scaling and Test Techniques," *Journal of the American Helicopter Society*, Vol. 66, No. 2, 2021, pp. 1–16. https://doi.org/10.4050/JAHS.66.022006.

[13] Niemiec, R., Ivler, C., Gandhi, F., and Sanders, F., "Multirotor Electric Aerial Vehicle Model Identification with Flight Data with Corrections to Physics-Based Models," *CEAS Aeronautical Journal*, Vol. 13, No. 3, 2022, pp. 575–596. https://doi.org/10.1007/s13272-022-00583-5.

[14] Wei, P., Lin, X., and Kong, Z., "System Identification of Wind Effects on Multirotor Aircraft," *International Journal of Intelligent Robotics and Applications*, Vol. 6, No. 1, 2022, pp. 104–118. https://doi.org/10.1007/s41315-021-00185-0.

[15] Gong, A., Sanders, F. C., Hess, R. A., and Tischler, M. B., "System Identification and Full Flight-Envelope Model Stitching of a Package-Delivery Octocopter," *AIAA Scitech 2019 Forum*, American Institute of Aeronautics and Astronautics, San Diego, CA, 2019, pp. 1–18. https://doi.org/10.2514/6.2019-1076.

[16] Simmons, B. M., "System Identification Approach for eVTOL Aircraft Demonstrated Using Simulated Flight Data," *Journal of Aircraft*, 2023, pp. 1–16. https://doi.org/10.2514/1.C036896.

[17] Bannwarth, J. X. J., Jeremy Chen, Z., Stol, K. A., MacDonald, B. A., and Richards, P. J., "Aerodynamic Force Modeling of Multirotor Unmanned Aerial Vehicles," *AIAA Journal*, Vol. 57, No. 3, 2019, pp. 1250–1259. https://doi.org/10.2514/1.J057165.

[18] Sun, S., de Visser, C. C., and Chu, Q., "Quadrotor Gray-Box Model Identification from High-Speed Flight Data," *Journal of Aircraft*, Vol. 56, No. 2, 2019, pp. 645–661. https://doi.org/10.2514/1.C035135.

[19] Bangura, M., "Aerodynamics and Control of Quadrotors," Ph.D. thesis, The Australian National University, Feb. 2017.

[20] Bristeau, P.-J., Martin, P., Salaun, E., and Petit, N., "The Role of Propeller Aerodynamics in the Model of a Quadrotor UAV," *2009 European Control Conference (ECC)*, IEEE, Budapest, 2009, pp. 683–688. https://doi.org/10.23919/ECC.2009.7074482.

[21] Nguyen, N., and Webb, B., "Analytical Flight Dynamic Model Development for eVTOL Aircraft," *AIAA SciTech 2025 Forum*, American Institute of Aeronautics and Astronautics, Orlando, FL, 2025, pp. 1–28. https://doi.org/10.2514/6.2025-0657.

[22] Fay, G., "Derivation of the Aerodynamic Forces for the Mesicopter Simulation," Stanford University, Feb. 2001. URL https://www.semanticscholar.org/paper/Derivation-of-the-Aerodynamic-Forces-for-the-Fay/f7a8f5ee403af857c9fa6db885b26401a58cd958.

[23] "High-fidelity Unmanned Multirotor Flight Dynamics Simulation for Off-nominal Conditions," NASA Technology Transfer Program, https://software.nasa.gov/software/LAR-19479-1, Accessed 20 May 2023.

[24] Montgomery, D. C., *Design And Analysis of Experiments*, 8th ed., John Wiley & Sons, Inc., Hoboken, NJ, 2013.

[25] Myers, R. H., Montgomery, D. C., and Anderson-Cook, C. M., *Response Surface Methodology: Process and Product Optimization Using Designed Experiments*, 4th ed., John Wiley & Sons, 2016.

[26] Johnson, W., *Helicopter Theory*, Princeton University Press, Princeton, N. J, 1980.

[27] Leishman, J. G., *Principles of Helicopter Aerodynamics*, 2nd ed., Cambridge University Press, Cambridge, 2006.

[28] Foster, J. V., and Hartman, D., "High-Fidelity Multi-Rotor Unmanned Aircraft System (UAS) Simulation Development for Trajectory Prediction Under Off-Nominal Flight Dynamics," *17th AIAA Aviation Technology, Integration, and Operations Conference*, American Institute of Aeronautics and Astronautics, Denver, Colorado, 2017, pp. 1–19. https://doi.org/10.2514/6.2017-3271.

[29] Khan, W., and Nahon, M., "Toward an Accurate Physics-Based UAV Thruster Model," *IEEE/ASME Transactions on Mechatronics*, Vol. 18, No. 4, 2013, pp. 1269–1279. https://doi.org/10.1109/TMECH.2013.2264105.

[30] Morris, D., and Pretty, C., "An Experimental Study of Drag Coefficients of a Quadrotor Airframe," *Volume 7: 19th IEEE/ASME International Conference on Mechatronic and Embedded Systems and Applications (MESA)*, American Society of Mechanical Engineers, Boston, Massachusetts, USA, 2023, p. V007T07A019. https://doi.org/10.1115/DETC2023-114020.

[31] Chintalapati, S., Rock, S., and Habchi, S., "Unsteady Aerodynamics of a Rapidly Tumbling Bluff Body," *37th Aerospace Sciences Meeting and Exhibit*, American Institute of Aeronautics and Astronautics, Reno,NV,U.S.A., 1999, pp. 1–10. https://doi.org/10.2514/6.1999-659.

[32] Caprace, D.-G., Ning, A., Chatelain, P., and Winckelmans, G., "Effects of Rotor-Airframe Interaction on the Aeromechanics and Wake of a Quadcopter in Forward Flight," *Aerospace Science and Technology*, Vol. 130, 2022, p. 107899. https://doi.org/10.1016/j.ast.2022.107899.

[33] Barcelos, D. F., Bramesfeld, G., Isaac, B., and Waslander, S., "Physics-Based Approach to Multirotor Vehicle Flight-Dynamics Prediction," *AIAA AVIATION 2021 FORUM*, American Institute of Aeronautics and Astronautics, VIRTUAL EVENT, 2021, pp. 1–15. https://doi.org/10.2514/6.2021-2532.

[34] Wolkovitch, J., "Analytical Prediction of Vortex-Ring Boundaries for Helicopters in Steep Descents," *Journal of the American Helicopter Society*, Vol. 17, No. 3, 1972, pp. 13–19. https://doi.org/10.4050/JAHS.17.13.

[35] Khalil, H. K., *Nonlinear Systems*, 3$^{\text{rd}}$ ed., Prentice Hall, Upper Saddle Ridge, New Jersey, 2002.

[36] "Design-Expert®," Version 13, Stat-Ease, Inc., https://www.statease.com/software/design-expert/, Accessed 21 May 2023.

[37] Goos, P., and Jones, B., *Optimal Design of Experiments: A Case Study Approach*, John Wiley & Sons, West Sussex, United Kingdom, 2011.

[38] Anderson, M. J., and Whitcomb, P. J., *RSM Simplified: Optimizing Processes Using Response Surface Methods for Design of Experiments*, 2$^{\text{nd}}$ ed., CRC Press, Boca Raton, FL, 2017. https://doi.org/10.1201/9781315382326.

[39] Simmons, B. M., "Advances in Aero-Propulsive Modeling for Fixed-Wing and eVTOL Aircraft Using Experimental Data," Ph.D. thesis, Virginia Polytechnic Institute and State University, Blacksburg, VA, Apr. 2023.

[40] Jategaonkar, R. V., *Flight Vehicle System Identification: A Time-Domain Methodology*, 2$^{\text{nd}}$ ed., Progress in Astronautics and Aeronautics, American Institute of Aeronautics and Astronautics, Inc., Reston, Virginia, 2015.

[41] Young, H. D., *Statistical Treatment of Experimental Data: An Introduction to Statistical Methods*, McGraw-Hill, New York, 1962.

[42] Bar-Shalom, Y., Li, X.-R., and Kirubarajan, T., *Estimation with Applications to Tracking and Navigation*, John Wiley and Sons, Inc., New York, 2001.